Characterization of the metalloproteases meprin α and meprin β within the protease web

Dissertation

zur Erlangung des Doktorgrades

der Mathematisch-Naturwissenschaftlichen Fakultät

der Christian-Albrechts-Universität

zu Kiel

vorgelegt von

Claudia Broder

Kiel, August 2013

Dekan: Prof. Dr. Wolfgang J. Duschl

Referent/in: Prof. Dr. Rose-John

Korreferent/in: Prof. Dr. Roeder

Tag der mündlichen Prüfung: 25.09.2013

Zum Druck genehmigt: 25.09.2013

Preface

This dissertation has been prepared partly cumulative. The data obtained in the presented work has been described in detail in five publications, which are attached to the end of the thesis.

1. Proteomic analyses reveal an acidic prime side specificity for the astacin metalloprotease family reflected by physiological substrates.
Becker-Pauly C, Barré O, Schilling O, Auf dem Keller U, Ohler A, **Broder C**, Schütte A, Kappelhoff R, Stöcker W, Overall CM.
Mol Cell Proteomics. 2011 Sep;10(9):M111.009233.

2. Structural basis for the sheddase function of human meprin β metalloproteinase at the plasma membrane.
Arolas JL, **Broder C**, Jefferson T, Guevara T, Sterchi EE, Bode W, Stöcker W, Becker-Pauly C, Gomis-Rüth FX.
Proc Natl Acad Sci U S A. 2012 Oct 2;109(40):16131-6.

3. The substrate degradome of meprin metalloproteases reveals an unexpected proteolytic link between meprin β and ADAM10.
Jefferson T, Auf dem Keller U, Bellac C, Metz VV, **Broder C**, Hedrich J, Ohler A, Maier W, Magdolen V, Sterchi E, Bond JS, Jayakumar A, Traupe H, Chalaris A, Rose-John S, Pietrzik CU, Postina R, Overall CM, Becker-Pauly C.
Cell Mol Life Sci. 2013 Jan;70(2):309-33.

4. The metalloproteases meprin α and meprin β: unique enzymes in inflammation, neurodegeneration, cancer and fibrosis.
Broder C, Becker-Pauly C.
Biochem J. 2013 Mar 1;450(2):253-64.

5. The Metalloproteases Meprin α and Meprin β are C- and N-procollagen Proteinases Important for Collagen Assembly and Tensile Strength.
Broder C, Arnold P, Vadon-Le Goff S, Konerding MA, Bahr K, Müller S, Overall CM, Bond JS, Koudelka T, Tholey A, Hulmes DJ, Moali C, Becker-Pauly C.
Proc Natl Acad Sci U S A. 2013 in press.

In the following, most relevant results from the publications 1-5 are briefly described and unpublished data are illustrated in detail.

Table of Contents

List of Figures

List of Tables

Abstract

Fibrillar collagen type I is the most abundant protein in human body and essential for the formation and strength of bone, skin, and tendon. The assembly of collagen fibrils is initiated by proteolytic enzymes which cleave off the propeptides of procollagen I. Hence, mutations in collagen genes and dysregulation of procollagen proteinase activity are the main causes of pathological disorders in collagen fibril formation. Here I demonstrate that the metalloproteases meprin α and meprin β are the only enzymes known so far capable of releasing the C- as well as the N-propeptides from type I procollagen both *in vitro* and *in vivo* thereby inducing the assembly of collagen fibrils. Meprin cleavage sites were found to be the same or in close proximity to those for the N-proteinase ADAMTS-2 and the C-proteinase BMP-1. Skin lysates from meprin α and meprin β knockout mice revealed smaller amounts of the mature collagen I compared to wild-type controls. As a consequence, meprin α and meprin β knockout mice exhibited significantly reduced collagen deposition in skin and an impaired arrangement of dermal collagen fibrils. This resulted in a markedly decreased tissue tensile strength. As a compensatory effect to partly offset the loss of procollagen proteinase activity in meprin knockout mice, expression of gene coding for bone morphogenetic protein-1/mammalian tolloid (BMP-1/mTLD) was significantly increased in these animals. These data demonstrate that meprin α and meprin β induce collagen fibril formation *in vitro* and *in vivo* and contribute to the integrity of connective tissue in skin. They regulate the collagen deposition in skin and might therefore be promising therapeutic targets to limit fibrosis.

Zusammenfassung

Fibrilläre Kollagene stellen die wichtigsten Proteine des Organismus dar. Sie sind die strukturgebenden Proteine von Haut, Knochen und Sehnen. Während der Synthese des Kollagens findet eine post-translationale Modifizierung des Prokollagens durch Proteasen statt, die die Propeptide abspalten. Durch das Fehlen der Propeptide sind Kollagenmoleküle in der Lage, sich zu langen Fibrillen aneinanderzulagern und es kommt zur Kollagenassemblierung. Im Rahmen dieser Dissertation konnte ich zeigen, dass die Metalloproteasen Meprin α und Meprin β die bisher einzigen bekannten Enzyme sind, die in der Lage sind, sowohl das C- als auch das N-Propeptid vom Prokollagen I *in vitro* und *in vivo* abzuspalten. Diese enzymatische Spaltung geht mit der Fibrillenbildung einher, die im Elektronenmikroskop beobachtet werden konnte. Konsequenterweise zeigen Meprin α und Meprin β Knockout-Mäuse signifikante Defekte bei der Integrität des Bindegewebes. Durch das Fehlen der C- und N-Proteinaseaktivität in Meprin Knockout-Mäusen kann weniger reifes Kollagen gebildet werden als in wildtypischen Kontrollmäusen. Histologische Untersuchungen der Haut haben ergeben, dass die Kollagenschicht dieser Meprin Knockout-Mäuse signifikant vermindert ist und die Kollagenfasern in der Haut dieser Mäuse weniger dicht gepackt, ungeordnet und kleiner im Durchmesser sind, woraus eine stark reduzierte Reißfestigkeit der Haut resultiert. Um das Fehlen der Prokollagen-Proteinaseaktivität zu kompensieren, werden die für das *bone morphogenetic protein-1/mammalian tolloid* (BMP-1/mTLD) codierenden Gene in diesen Mäusen stark überexpremiert.

In der vorliegenden Arbeit zeige ich, dass sowohl Meprin α als auch Meprin β die Kollagenassemblierung *in vitro* und *in vivo* induzieren und somit an der Stabilität des Bindegewebes beteiligt sind. Sie regulieren die Kollageneinlagerung in der Haut und sind aus diesem Grund vielversprechende therapeutische Targets in der Fibrose.

1 Introduction

Proteases are essential enzymes in almost all biological processes in health and disease, irreversibly modulating the proteome. The controlled regulation of proteolysis is crucial for the maintenance of tissue homeostasis and physiological balance. In humans, 578 proteolytic enzymes are encoded by about 2% of all genes [1,2]. The precise physiological function of the majority of these enzymes remains unknown.

1.1 Meprin metalloproteases

The metalloproteases meprin α and meprin β were discovered over 30 years ago, but little was known about their biological activity until recently. Meprins belong to the astacin family of metalloproteases, comprising only six members in humans. This family is characterized by a conserved zinc-binding motif (HExxHxxGxxHxxxRxDR) and the so called Met-turn in close proximity to the active site that includes a tyrosine residue as a fifth zinc ligand [3,4]. Meprin α and meprin β are expresses as highly glycosylated disulfide linked homo-dimers that require enzymatic removal of the N-terminal propeptide by serine proteases to gain full activity [3,5,6,7,8]. Meprins exhibit unique domain compositions among astacins comprising a N-terminal signal peptide directing the polypeptide chain to the endoplasmic reticulum, followed by a N-terminal propeptide, an astacin-like protease domain, a MAM (meprin A5 protein tyrosine phosphatase μ) and a TRAF (tumour-necrosis-factor-receptor-associated factor) domain, both of which are known to mediate protein–protein interactions, an EGF (epidermal growth factor)-like domain, a transmembrane domain, and a C-terminal cytosolic tail (Fig. 1A) [3]. In contrast to meprin β, meprin α contains an additional “inserted” domain, which includes a furin

cleavage site. The cleavage by furin results in the loss of the EGF-like, transmembrane and cytosolic domains, and in a subsequent release of the soluble enzyme into the extracellular space where it further oligomerizes non-covalently, building huge complexes in the mega-Dalton range [3,6,9]. This makes meprin α the largest secreted protease known to date. Lacking the “inserted” domain, meprin β remains tethered to the cell membrane as a dimeric type I integral protein, but it can be released from the cell surface by ADAM10 and ADAM17 [3,10,11].

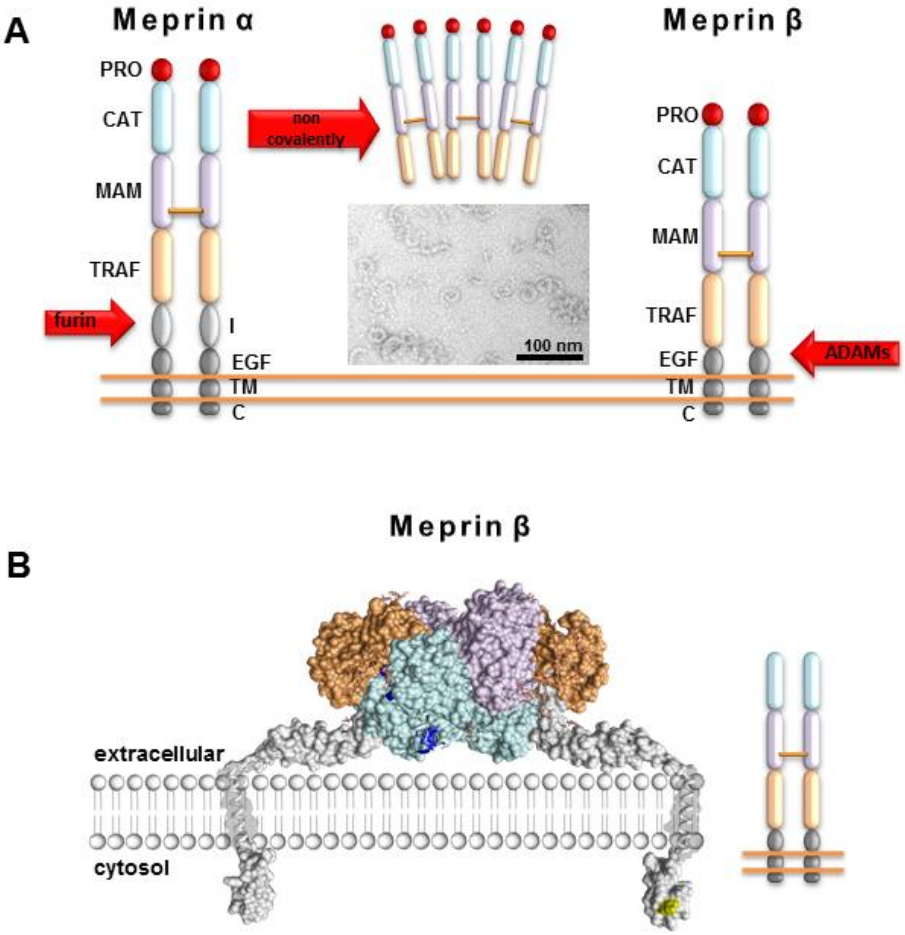

Figure 1: Oligomeric structure of human meprin metalloproteases [3].

(A) Meprin α and meprin β are multi-domain enzymes, expressed as zymogens with a N-terminal propeptide (PRO) that must be removed proteolytically to gain full activity, followed by the protease domain (CAT). Meprins build dimers linked by one intermolecular disulfide bond between the MAM domains. Only meprin α contains an inserted domain (I) which is cleaved by furin during the secretory pathway. This results in secretion of soluble meprin α which further oligomerizes to large non-covalently linked complexes, as visualized by electron microscopy of the purified recombinant enzyme. Meprin β predominantly remains membrane-bound, but it can be shed from the cell surface by ADAM10 and ADAM17. [3]. (B) Model of the membrane-bound form of meprin β and its orientation at the cell surface. EGF-like, transmembrane and cytosolic domains are displayed in grey, and phosphorylation sites are in yellow. Positively charged residues within the active-site cleft of the catalytic domain are shown in dark blue [3].

The recently solved crystal structure of meprin β (Fig. 1B) suggests possible mechanisms of activation, substrate recognition and binding [12]. This knowledge is fundamental especially for the design of specific inhibitors however the structure does not reveal the physiological function of a protease.

1.2 The meprin degradome

In recent years new technologies have been employed to investigate the role of meprins in a physiological and pathological context. The central challenge for the characterization of a protease function is the identification of its substrate repertoire. Meprins have been implicated in angiogenesis, cancer, and inflammation [3]. However, it has not been completely understood which meprin mediated proteolytic events were responsible for these effects. Initially, the application of proteomics techniques allowed the characterization of the meprin degradome in a cellular context. Using the mass spectrometry based proteomics technique TAILS (terminal affinity isotope labeling of substrates) [13], which enables a direct identification of neo-N-termini generated by proteolysis, more than 100 extracellular proteins were identified as substrates of meprin α and meprin β consisting of growth factors, receptors, hormones, proteases, inhibitors and other proteins (Fig. 2) [10].

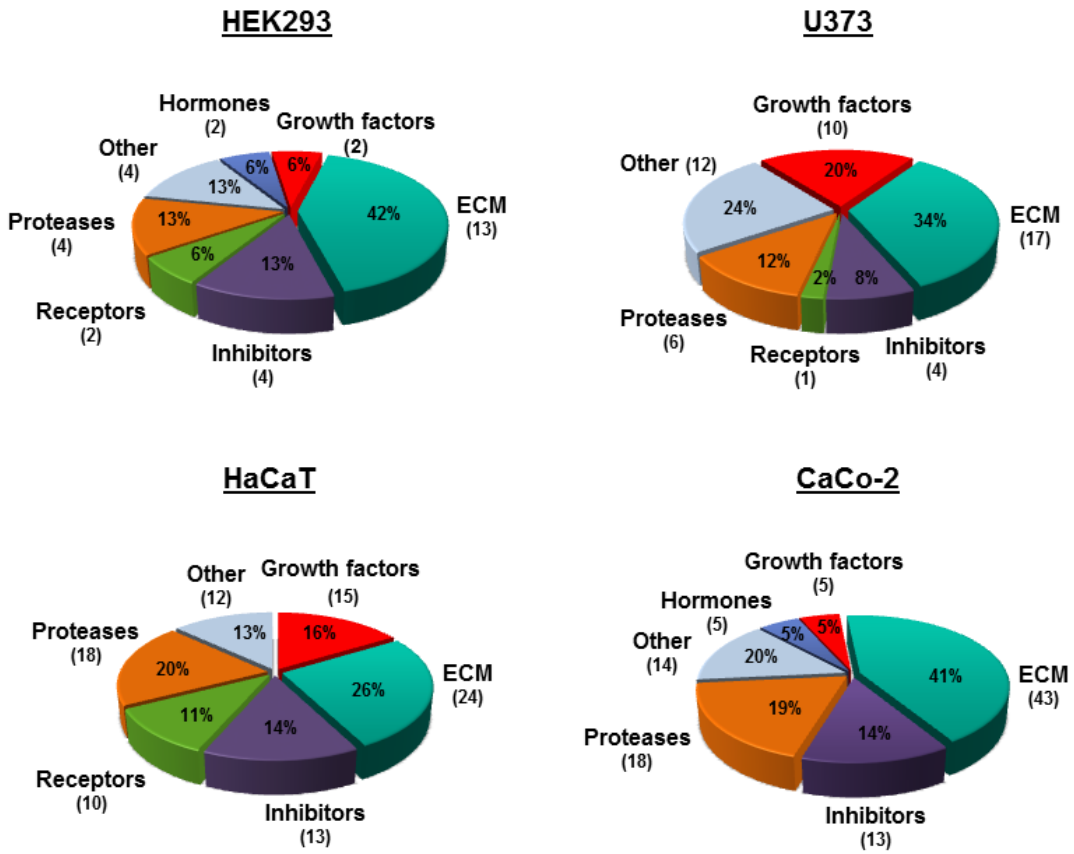

Figure 2: Categorization of meprin substrates identified using TAILS.

Employing TAILS in the human cell lines HEK293, U373, HaCaT and CaCo-2 novel substrates were identified including inhibitors, receptors, proteases and other proteins with uncharacterized functions. Numbers of identified substrates are given in parentheses [10].

The amyloid precursor protein (APP) was identified by TAILS as a putative substrate for meprin β and Bien et al. confirmed that meprin β sheds APP from the cell surface, releasing Aβ peptides similarly to the known β-site APP-cleaving enzyme 1 (BACE-1) [14]. These Aβ peptides accumulated in amyloid plaques are neurotoxic and were proposed to have a pathological effect on the progression of Alzheimer's Disease (AD) [3,15]. Additionally, meprin β cleaves the N-terminus of APP *in vivo* releasing N-terminal fragments of 22 and 11 kDa (APP22 and APP11) [16]. The latter was previously observed in human brain lysates [17] suggesting the physiological relevance of meprin β in neurobiology. On the other hand, using TAILS

it was possible to identify the α-secretase ADAM10 as a substrate for meprin β [10]. It has been shown that meprin β activates the α-secretase ADAM10 through cleavage of the propeptide. This leads to the activation of ADAM10 which is than able to shed APP by cleaving within the Aβ region, liberating the soluble ectodomain sAPPα, thus preventing the formation and aggregation of neurotoxic Aβ peptides (Fig. 3) [18,19]. Additionally, when active ADAM10 is able to shed the membrane bound meprin β from the cell surface, thereby releasing it into the extracellular space where it can cleave other soluble substrates. Therefore, the unbiased proteomics approach TAILS enabled to discover a possible proteolytic web of meprin β in a pathological context (Fig. 3). The network of interactions depends on the activities of proteases, their substrates and inhibitors [20]. Meprins themselves are expressed as zymogens and the enzymatic cleavage of the N-terminal propeptide by serine proteases leads to their activation. Interestingly, a range of serine protease inhibitors such as elafin, secretory leukocyte protease inhibitor (SLPI), and Lympho-epithelial Kazal-type-related inhibitor (LEKTI) were found to be cleaved by meprins, increasing the complexity of the proteolytic web (Fig. 3) [10].

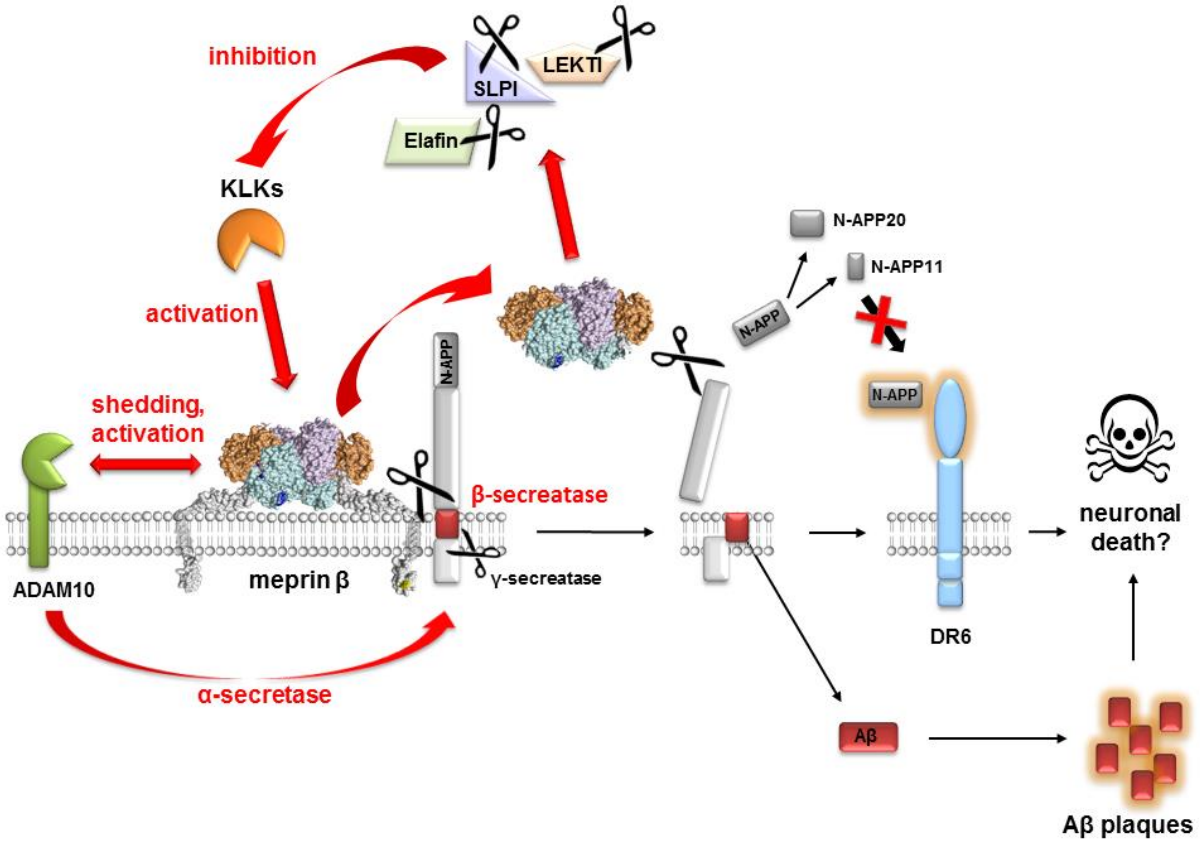

Figure 3: Meprin β within the proteolytic web.

Membrane-bound meprin β generates Aβ peptides which can form neurotoxic Aβ plaques [14]. On the other hand meprin β interacts with ADAM10, the constitutive α-secretase [10]. Shedding by ADAM10 leads to soluble meprin β, which is no longer capable of cleaving at the β-secretase site, but still releases N-APP fragments that exhibit no neurotoxic capacity and are rather protective against death receptor 6 (DR6)-mediated neuronal death [16]. Human tissue KLKs are activators of meprin β [5] and their activity is regulated through the serine protease inhibitors elafin, SLPI and LEKTI, which can also be cleaved by meprin β [10].

1.3 The proteolytic web in skin

The complexity of the proteolytic network becomes even more apparent in skin, where meprin α and meprin β are differentially expressed. The skin is the largest organ of the body, representing a barrier against external physical, chemical and biological influences due to its complex organization in distinct layers [3,21]. Both meprins are constitutively expressed in human epidermis [22]. Due to their different roles in keratinocyte differentiation meprin α and meprin β are expressed in different layers where they modulate the extracellular matrix (ECM), thereby contributing to the homeostasis in skin. The extracellular matrix plays an essential role in organizing

tissues, defining their shapes or in presenting growth factors. Meprin α is exclusively expressed in the stratum basale, where it might be activated by plasmin [7] and where it promotes proliferation of human keratinocytes. A range of growth factors, hormones, proteases and inhibitors were identified in human keratinocytes using TAILS as possible substrates for meprin α [10]. Additionally, *in vitro* studies demonstrated the processing of several components of the basal membrane such as collagen IV, fibronectin, laminin and nidogen by meprin α, thus contributing to the ECM remodeling during cell proliferation and migration [10,23,24].

In contrast to meprin α, meprin β is expressed in the upper layer of the epidermis, the stratum granulosum, where it can be activated by KLK (kallikrein related peptidases) 4, 5 and 8 [5,22]. Upon activation, meprin β is able to cleave cell-adhesion molecules such as E-cadherin and desmogleins thereby inducing terminal differentiation and might be involved in cornification and desquamation [10,25]. Additionally, Ohler et al. demonstrated the ability of meprin β to process proKLK7 only two amino acids N-terminal from the activation site, subsequently leading to an enhanced activation of proKLK7 [5]. On the other hand, meprin β cleaves a range of serine protease inhibitors which directly modulate KLK activity (Fig. 3) [10]. This proteolytic web in the epidermis is further completed by the ability of meprin β to activate ADAM10, an enzyme known to be essential for epidermal homoeostasis [26]. The maintenance of the epidermal homeostasis is fundamental for the barrier function of the skin and dysregulation is often associated with pathological consequences as in the diseases *psoriasis vulgaris* and the Netherton syndrome.

1.4 The role of meprins in collagen assembly

The basal keratinocyte layer of the epidermis is attached to a basement membrane, which overlies the connective tissue layer known as the dermis. Dermal ECM consists of fibrillar collagens type I and III which are the main sources of mechanical strength and stability of the skin. The remodeling of the ECM is an important process in the homeostasis of connective tissue and combines synthesis, deposition, and degradation of ECM molecules [27]. Fibrillar collagens such as types I, II, and III are secreted as precursor molecules, the procollagens, and undergo a range of post-translational modifications upon the collagen fibril is built and deposited in the ECM. The key step in the formation of collagen fibrils is the proteolytic removal of the globular N- and C-terminal propeptides, thereby exposing short non-helical telopeptides at both the N- and the C-termini [28,29,30,31]. Consequently, these mature collagen molecules spontaneously assemble into collagen fibrils while the telopeptides are covalently cross-linked stabilizing the mature collagen fibrillar structure (Fig. 4) [29]. The N-propeptide of procollagen I is cleaved off by the members of the ADAMTS (a disintegrin and metalloproteinase with thrombospondin motifs) family, ADAMTS-2, -3 and -14, while the procollagen I C-proteinase activity is due to BMP-1 (bone morphogenetic protein-1) and related tolloid-like proteinases [32,33,34,35]. However, ADAMTS or BMP-1 knockout mice exhibit residual procollagen I N- or C-proteinase activity and are able to deposit collagen fibrils in skin [32,36]. This indicates that there are additional proteases which mediate cleavage *in vivo*.

It has been shown that both, meprin α and meprin β cleave off the C-propeptides from the fibrillar procollagen III *in vitro* at exactly the same site and even more efficiently than the procollagen C-proteinase BMP-1 [37]. Additionally, proteomic analyses using TAILS in a cell culture system revealed cleavage in

procollagen α2(I) by both meprin α and meprin β [10]. This cleavage would lead to the removal of the C-propeptide of the α2 chain of type I procollagen and induce collagen fibril formation. The removal of the C-propeptide from fibrillar collagens is the initial step in collagen fibril assembly, suggesting that meprins are involved in procollagen turnover and might contribute to collagen deposition in skin. This was further supported by the fact that both meprins are overexpressed in human dermal fibroblasts of fibrotic tumors (keloids) [37] where collagen synthesis, maturation and deposition take place.

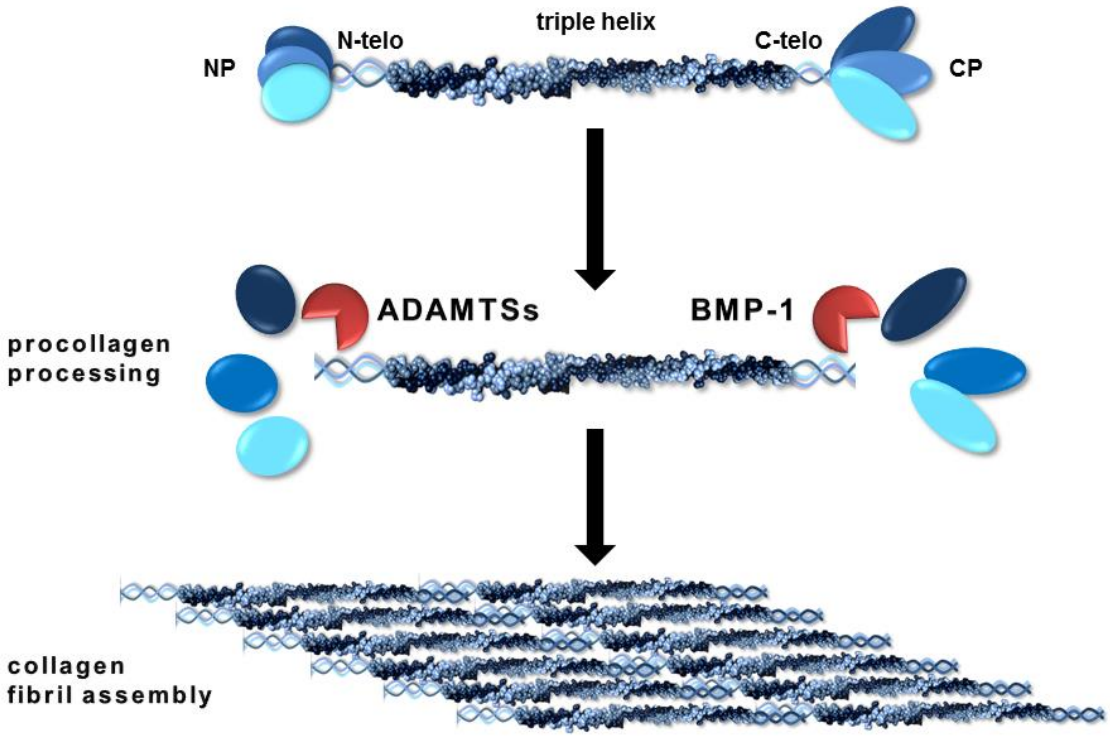

Figure 4: Procollagen I maturation and fibril formation.

Fibrillar collagens secreted as procollagens containing a central triple helical domain, flanked by lineal N- and C-telopeptides (N-telo, C-telo), and globular N- and C-propeptides (NP, CP). Collagen fibril formation is induced by the proteolytic removal of the propeptides by members of the ADAMTS (a disintegrin and metalloproteinase with thrombospondin motifs) family, ADAMTS-2, -3 and -14 and BMP-1 (bone morphogenetic protein-1). The release of the mature collagen molecules leads to the spontaneous assembly into collagen fibrils while the telopeptides are covalently cross-linked stabilizing the fibrillar structure.

1.5 Meprins as therapeutic targets

The implication of meprins in many pathological processes such as neurodegeneration, inflammation, cancer and fibrosis provides evidence that these enzymes might be promising therapeutic targets [3]. Initially the application of the proteomics approach PICS (proteomic identification of protease cleavage sites) contributed to the understanding of the cleavage specificity of meprin α and meprin β. Becker-Pauly et al. demonstrated the striking preference for negatively charged amino acid residues in the P1' position for meprin α and meprin β [38]. This cleavage specificity was concordant with many cleavage sites generated by meprins *in vitro* and *in vivo*. According to the crystal structure of meprin β, negatively charged amino acid residues exhibit the ideal distribution for the interaction with the positively charged arginine residues Arg^{516} and Arg^{567}, both part of the TRAF domain of meprin β and extended into the active site cleft [3,12]. This knowledge might be beneficial for the development of specific peptide-inhibitors as small inhibitory compounds for the regulation of meprin activity in pathological conditions as fibrosis.

This study demonstrates that meprin α and meprin β are the first known C- and N-proteinases for type I procollagen *in vitro* and *in vivo*. Consequently, meprin α and meprin β knockout mice exhibit a reduced collagen I maturation and deposition in skin resulting in a decreased tensile strength of the skin. Since meprins are overexpressed in the dermis of human fibrotic skin, it is evident that the regulation of meprin activity in this pathologic condition might allow for the generation of a novel therapeutic approach to limit collagen deposition in skin.

2 Material and Methods

2.1 Cleavage of human procollagen I heterotrimer by meprin α, meprin β, and BMP-1/PCPE-1

Recombinant human meprin α and meprin β were expressed in baculovirus infected insect cells and purified and activated as described [6,22]. Full length human BMP-1, recombinant human PCPE-1 (procollagen C-proteinase enhancer-1), and recombinant human procollagen I heterotrimer were kindly provided by David Hulmes and Catherine Moali (Tissue Biology and Therapeutic Engineering Unit, CNRS, University of Lyon, France). 40 nM human procollagen I heterotrimer was incubated with 0.3 nM recombinant proteinase, in a total volume of 50 µl, for 1, 10, 30, 60 or 90 min at 37°C, in reaction buffer (20 mM HEPES, pH 7.4 for meprin α and meprin β and 50 mM Tris pH 7.4, 150 mM NaCl, 5 mM $CaCl_2$, 0.02% Brij35 for BMP-1/PCPE-1). In the case of BMP-1, PCPE-1 was present at equimolar concentrations with respect to the substrate. Proteins were separated by sodium dodecyl sulfate-polyacrylamide gel electrophoresis (SDS-PAGE) under reducing conditions and transferred onto PVDF-membranes by electroblotting. For immunodetection specific polyclonal antibodies raised against epitopes within the procollagen α1(I) (N-propeptide (LF-39), the C-propeptide (LF-41), and the C-telopeptide (LF-68) [39], kind gift from Larry W. Fisher (National Institute of Health/NIDCR, Bethesda, USA) were used.

Mass spectrometry based identification of meprin cleavage sites in human procollagen α1(I) and α2(I) was performed by the Z2 Unit of the CRC875 as described in [40].

2.2 *De novo* fibril formation assay using procollagen I heterotrimers

For transmission electron microscopy, 0.1 mg/ml recombinant procollagen was incubated with 15 nM recombinant proteinase for 60 min at 37°C in reaction buffer (20 mM HEPES, pH 7.4 for meprin α and meprin β and 50 mM Tris pH 7.4, 150 mM NaCl, 5 mM $CaCl_2$, and 0.02% Brij35 for BMP-1/PCPE-1). Staining of the samples and transmission electron microscopy was performed by Philipp Arnold (Institute of Zoology, Johannes Gutenberg-University, Mainz, Germany) as described in [40].

2.3 Experimental animals and determination of the genotype

12 to 16 week old male mice on a congenic C57BL/6 background were used for this study. Three genotypes were studied, wild-type (WT) mice and meprin α and meprin β knockout mice in which the meprin genes were ablated [41]. Mice were maintained on a 12-hour light–dark cycle, with food and water *ad libitum*. Genotype of the mice was determined by PCR. Tail biopsies were incubated overnight at 55°C with gentile agitation in 200 µl Direct PCR Lysis Buffer (PEQLAB Biotechnology GmbH) with proteinase K added to 0.1 mg/ml final concentration. Proteinase K was heat inactivated at 85°C for 45 minutes, samples were stirred and DNA was then used for PCR analyses to determine the genotype (Tab. 1). PCR primers (Invitrogen) were used to amplify the neomycin cassette containing the stop codon [41] as well as the whole modified exon 7 of *Mep1a* or *Mep1b* gene. Amplified DNA was separated on a 0.8% agarose gel. PCR primers mepa18-forward and mepa9-reverse generated 3.1 kb big fragments amplifying the WT exon 7 of the *Mep1a* gene and 4.3 kb big fragments, when the neomycin cassette was inserted. Using the primer mepb9Ge2-forward and mepb8Ge2-reverse, which flank the exon 7 of the *Mep1b* gene, PCR products were 2.36 kb in size when exon 7 was not modified and 3.96 kb when exon 7 contained the neomycin cassette. Since the signal for the modified exon was very

weak in *Mep1b*$^{+/-}$ and *Mep1b*$^{-/-}$ samples, additionally PCR primers flanking only the 131 bp long neomycin cassette (neo-forward and neo-reverse) were used to confirm the genotype (Tab. 1).

Table 1: PCR Primers used for determination of the genotype of mice.

Primer	**Sequence**
mepa18-forward	5'-GCG AGG GAC CTC CCA TGA TAA ACT TAG G-3'
mepa9-reverse	5'-CCC CTG GAG TCT GTC TAG TAG CCA TCA TC-3'
mepb9Ge2-forward	5'-GCC TTG GTC GTC CG GAGA AGC TAA CTA CTC-3'
mepb8Ge2-reverse	5'-ACC AGG CTA CTT AGC TCC CTG TTA TTG-3'
neo-forward	5'-TCA AGG GCA GTG GGT GCT GGT 3'
neo-reverse	5'-ATG CCA GAA TCC CAG GGC GTG-3'

Table 2: Pipetting scheme for genotyping PCR.

Reagent	**Volume for *Mep1a*-PCR**	**Volume for *Mep1b*-PCR**
DNA Template	2 µl	1 µl
10 x Taq Polymerase Buffer	5 µl	3 µl
dNTP Mix (2mM)	5 µl	1 µl
forward primer (10 µM)	1 µl	0.3 µl
reverse primer (10 µM)	1 µl	0.3 µl
ddH2O	add 50 µl	add 30 µl

Program for *Mep1a*-PCR.

Initial denaturation	95°C	2 min	
Denaturation	98°C	20 sec	30 cycles
Annealing	60°C	30 sec	
Elongation	72°C	4.5 min	
Final elongation	72°C	4.5 min	

Program for *Mep1b*-PCR.

Initial denaturation	95°C	2 min	
Denaturation	98°C	20 sec	35 cycles
Annealing	64°C	30 sec	
Elongation	68°C	6 min	
Final elongation	68°C	6 min	

2.4 Skin lysate preparation

Dorsal skin was shaved, dissected and pulverized into powder in a liquid nitrogen-cooled pestle and mortar. Skin lysates were prepared by adding lysis buffer (50 mM Tris/HCl, pH 6.8, 150 mM NaCl, 1% TritonX100, 1% SDS, 2 mM EDTA) containing a cocktail of Complete^{TM} protease inhibitors (Roche Applied Science) for 24 h at 4°C. Skin homogenates were then centrifuged at 13,000 rpm at 4°C for 30 min. The supernatant was used for Western blot analysis as described in 2.1. Since the anti-N-propeptide antibody (LF-39) did not cross-react with murine procollagen I it was not used for detection of collagen in murine skin lysates. Western blots were quantified by using ImageJ 1.47 [40].

2.5 Histological analyses

Biopsies from dorsal skin of WT (n=6), *Mep1a*$^{-/-}$ (n=6), and *Mep1b*$^{-/-}$ (n=6) mice were fixed 24-48 h in neutral buffered formalin (4%). Paraffin embedding and azan trichrome staining was performed by Kerstin Bahr (Institute of Anatomy, University Medical Center of the Johannes Gutenberg-University, Mainz, Germany) as described in [40]. The thickness of the collagen layer was measured by light microscopy (Axiophot, Zeiss) using the morphometry software Diskus 4.8 (Hilgers). The mean thickness of the different specimens was obtained taking the average of five measurements per section [40].

2.6 Tissue preparation for transmission electron microscopy of dermal fibrils

Skin samples from age-matched wild-type, *Mep1a*$^{-/-}$, and *Mep1b*$^{-/-}$ animals were fixed with 2.5% glutaraldehyde in 0.1 M cacodylate buffer pH 7.5 with 0.1 M sucrose, followed by post-fixation with 2% osmium tetroxide. After dehydration in a graded series of ethanol solutions (30, 50, 70, 80, 90, 95, and 100%) samples were embedded in Araldite. Ultrathin sections (50 nm) (Ultracut S Microtome, Leica, Microsystems) were visualized using a Tecnai12 (FEI) electron microscope operating a LaB6 electron source. Images were taken by Philipp Arnold (Institute of Zoology, Johannes Gutenberg-University, Mainz, Germany) on a 4kx4k CCD camera (TVIPS). Average diameters (nm) were obtained by measuring fibrils from 3 WT (n=414), 3 *Mep1a*$^{-/-}$ (n=598), and 3 *Mep1b*$^{-/-}$ mice (n=414). Graphs were plotted using the software package R 2.13.0 [40].

2.7 Biomechanical testing of maximum skin tensile strength

Dorsal skin from wild-type (n=6) and aged-matched meprin α (n=6) and meprin β (n=6) knockout mice was carefully shaved; dissected, and pinned to avoid shrinking. All biopsies tested (3-4 per mouse and strain) had a defined hourglass form with a

width of 3 mm at the narrowest part, constituting a predefined breaking point. All skin specimens were orientated parallel to the spine and were kept moist with 0.9% isotone NaCl at room temperature. Specimens were held between the gripping jaws and were stretched at a constant rate of 3 mm/s, which resulted in load onset rates of less than 0.05 N/s. The end point was the ultimate load (in Newton, N) at which skin disruption occurred. A position encoder (WA300) was used to register the distance covered, and a force transducer for traction and compression (S2, maximum value 500 N) was used to quantify the power impacting on the skin. The resulting values were recorded by a multiple channel PC measuring device (Spider 8) and plotted as a distance-power curve (software, Catman 3.0; both from HBM Hottinger Baldwin Messtechnik). The mean maximum tensile strength for each mouse was obtained by averaging three to four measurements per animal [40].

2.8 RNA isolation, reverse transcription and quantitative real-time PCR

Total RNA was isolated from skin and primary fibroblasts of WT, meprin α, and meprin β knockout animals (n=3) using the GeneJET RNA Purification Kit (Fermentas, Thermo Scientific). Equal amounts of RNA (1 µg) were transcribed into complementary DNA in 25 µl reaction mixtures using RevertAid™ Transcriptase (200 U/ml), 10 mM nonspecific oligo d(T) primers, and 200 mM dNTPs (Fermentas, Thermo Scientific). The cDNA obtained was subjected to quantitative real-time PCR measurement in a 10 µl reaction, using the LightCycler480® Real-Time PCR System (Roche Applied Science) according to the manufacturer's instructions. The amplification reaction consisted of a hold of 10 min at 95°C then 45 cycles (10 sec/95°C, 30 sec/60°C). For assay design, the Universal ProbeLibrary System (http://qpcr.probefinder.com/roche3.html) was used to amplify intron spanning regions for the gene of interest. Relative amounts of target gene mRNA were

normalized to the housekeeping gene GAPDH (Glyceraldehyde-3-phosphate dehydrogenase). The following primers and probes were used:

Table 3: Primers and corresponding probes for quantitative real time PCR using the LightCycler480® Real-Time PCR System.

Primer	Sequence	Probe
BMP-1/mTLD_forward	5'-GCA CTA TGC CCG GAA CAC-3'	# 80
BMP-1/mTLD_reverse	5'-CCT CAT ACT TGG GAA CAA TGG-3'	
mTLL-1_forward	5'-AAA GAG TGC ACG TGG GTG AT-3'	# 72
mTLL-1_reverse	5'-AAC CTC AAA CTC ATT GAA GGC TA-3'	
mTLL-2_forward	5'-CAT GAG AAC GGA CAC GAC TG-3'	# 71
mTLL-2_reverse	5'-CCT CTG CAC TGC TGA TCT TG-3'	

For analysis of connective tissue associated genes a mouse fibrosis PCR array was used according to the manufacturer's instructions (SA Biosciences). ΔΔCp values were used to calculate the relative expression for each data point [40].

2.9 Collagenase activity of human recombinant MMP-1 *in vitro*

Human recombinant MMP-1 was a kind gift from Christopher Overall, UBC Vancouver, Canada [42]. 40 ng human recombinant pro-MMP-1 were activated with 1 mM p-aminophenylmercuric acetate (APMA) for 2 h at 37°C prior to or after incubation with 4.5 nM meprin α or meprin β. All activity assays were performed in 50 mM HEPES, pH 7.5 with 10 µM quenched fluorogenic peptide Mca-Pro-Leu-Gly-Leu-A2(Dnp)-Ala-Arg-NH_2 at 37°C and the fluorescence was detected over 120 min. Enzyme activity was measured with the fluorescent spectrometer Varioskan Flash

(Thermo Scientific) and data were analyzed using “SkanIt Software 2.4 for Varioskan Flash”. Proteolytic activity was calculated from the emission at 405 nm with an excitation at 320 nm [40].

2.10 Cleavage of recombinant human Hsp47 by meprin α and meprin β *in vitro*.

Human recombinant Hsp47 (heat shock protein 47), was kindly provided by Ulrich Baumann and Jan Gebauer (Institute of Biochemistry, University of Cologne, Germany). 5 µg human recombinant Hsp47 was incubated with 15 nM meprin α or meprin β, in a total volume of 10 µl for 1, 30, and 60 minutes at 37°C, in 20 mM HEPES buffer at pH 7.5, 7.0, 6.5 or 6.0. SDS-PAGE was performed under reducing conditions and subsequently stained with Coomassie solution. Collagen binding ELISA was performed by Jan Gebauer as described in [43].

2.11 *In vitro* activity of meprin α, meprin β and BMP-1

All activity assays were performed with 15 nM protease in 20 mM HEPES buffer, pH 7.5 with 10 µM quenched fluorogenic peptide (Genosphere Biotechnologies) at 37°C and the fluorescence was detected until protease saturation. All assays were performed in duplicates in a 96-well plate in a total volume of 100 µl. Fluorogenic peptides used for this study are listed in table 4. Enzyme activity was measured with the fluorescent spectrometer Infinite 200 PRO (TECAN) and data were analyzed using Magelan software version 7.1. Proteolytic activity was calculated from the emission at 405 nm with an excitation at 320 nm.

Table 4: Quenched fluorogenic peptides for determination of meprin β activity.

Substrate	Sequence
P1	Mca-Glu-Asp-Glu-Asp Glu-Asp-(Dnp)
P2	Mca-Glu-Glu-Glu-Glu-Glu-Glu-(Dnp)
P3	Mca-Asp-Asp-Asp-Asp-Asp-Asp-(Dnp)
P4	Mca-Tyr-Val-Ala-Asp-Ala-Pro-Lys-(Dnp)

Inhibition studies with the phosphinic meprin β inhibitor (PMI) (kind gift from Vincent Dive, CEA, Service d'Ingénierie Moléculaire des Protéines, Cedex, France) were performed with 1 nM meprin β in 20 mM HEPES buffer, pH 7.5 with 10 µM quenched fluorogenic substrate P4 (Tab. 4). 1-100 nM phosphinic meprin β inhibitor was incubated with active meprin β for 30 min at 37°C subsequently enzyme activity was measured.

2.12 Cell surface activity of meprin β

Equal amount of MDCK (Madin-Darby Canine Kidney Epithelial) cells stably transfected with wild-type human meprin β or the meprin β catalytically inactive mutant E90A was seeded in a 24-well plate and were grown in DMEM with 10% FCS until 90% confluence. Cell culture medium was removed and cells were rinsed once with PBS to remove traces of FCS. Cell surface activity of meprin β was determined in the presence or absence of 100 nM phosphinic meprin β inhibitor and 10 µM quenched fluorogenic peptide P1 (Tab. 4) in a total volume of 400 µl in FCS-free DMEM. Enzyme activity was calculated as described in 2.11.

2.13 Meprin β activity in kidney lysates

Kidneys from WT, *Mep1b*$^{-/+}$, and *Mep1b*$^{-/-}$ mice were pulverized into powder in a liquid nitrogen-cooled pestle and mortar. Kidney lysates were prepared by adding lysis buffer (1% TritonX100 in PBS, pH 7.4) containing a cocktail of Complete^{TM} protease inhibitors without EDTA (Roche Applied Science) for 30 min on ice. Kidney homogenates were then centrifuged at 13,000 rpm at 4°C for 30 min. The supernatant was used for determination of meprin β activity. Protein concentrations were determined using the BCA (bicinchoninic acid) assay (Fermentas, Thermo Scientific) with bovine serum albumin as standard. Meprin β activity was measured in 200 µg total protein in the presence or absence of 100 nM phosphinic meprin β inhibitor or 10 µM actinonin and 10 µM quenched fluorogenic peptide P1 (Tab. 4) as described in 2.11.

2.14 *In vitro* activity of KLK2, KLK4, and KLK7 and determination of IC_{50}

Recombinant human kallikrein-related peptidases (KLK) 2, 4 and 7 were a kind gift from Viktor Magdolen (Clinical Research Unit, Department of Obstetrics and Gynecology, Technical University of Munich, Germany). For all activity measurements 50 µg/ml protease (KLK2, KLK4, and KLK7) were used in 50 mM Tris/HCl buffer, pH 8.0, containing 100 mM NaCl and 0.005% Tween 20. All activity assays were performed in duplicates in a 96-well plate in a total volume of 100 µl. Activity of KLK2 and KLK4 was determined using the quenched fluorogenic peptide Z-Pyr-Gly-Arg-Mca (Peptide Institute Inc.). For KLK7 activity measurements the quenched fluorogenic peptide Suc-Leu-Leu-Val-Tyr-AMC (Peptide Institute Inc.) was applied. Rate of hydrolysis was monitored as described in 2.11.

For determination of the IC_{50} values of recombinant human $sAPP_{751}$, proteases were incubated for 10 min at 37°C with $sAPP_{751}$ (1 nM, 10 nM, 40 nM, 60 nM, 80 nM and

100 nM). Following addition of the appropriate substrate (60 µM Z-Pyr-Gly-Arg-Mca or 30 µM Suc-Leu-Leu-Val-Tyr-AMC), the rate of proteolysis was monitored as described in 2.11. IC_{50} was calculated by nonlinear regression analysis using the GraFit software version 4.0.

2.15 Generation of monoclonal antibodies against human meprin α

Generation of hybridoma-producing monoclonal antibodies (mAb) against human meprin α, purification and biotin labeling of the antibodies was performed by Achmad Trad (Z2 Unit of CRC875) as described in [44].

To investigate the specificity of the generated mAb, Western blot analyses were performed using 0.5 µg recombinant human proteases. Binding of mAb to native meprin α was analyzed by immunoprecipitation. 200 µl of cell culture medium from human colon carcinoma cell line CaCo-2 were incubated with 200 µl hybridoma medium containing mAb over night at 4°C. 50 µl Protein G Agarose-beads (Fermentas, Thermo Scientific) were added to precipitate the soluble meprin α. After final washing steps beads were heated in 3x sample loading buffer to elute immunoprecipitated proteins, which were then loaded on 10% SDS-gels. Proteins were separated by SDS-PAGE, and subsequently transferred on a PVDF membrane. PVDF membrane was blocked in 3% BSA in TBS (10 mM Tris/HCl, pH 7.6, 150 mM NaCl) for 1 h and then incubated with supernatants containing the mAb diluted at 1:100 in 3% BSA over night at 4°C. Blots were then incubated for 1 h with anti-mouse IgG POD conjugate. Protein bands were visualized by chemiluminescence using ECL.

2.16 Establishing a meprin α specific sandwich ELISA

For sandwich ELISA Microtiter plates (Nunc, Denmark) were coated with 10 µg/ml of purified antibody M41-14/M41-15 per well in coating buffer (0.5 M

carbonate/bicarbonate buffer, pH 9.6) and incubated over night at 4°C. Then, plates were washed using the washing solution (PBS, 0.1% BSA) and blocked with 1% BSA in PBS for 2 h at room temperature. 100 µl of human serum, cell culture medium or 4-3000 ng/ml meprin α was added and incubated for 2 h at room temperature. Blank control was performed with PBS. The plates were washed with washing solution and the antigen was detected by 100 µl of biotinylated antibody M41-14/M41-15 at a final concentration of 1 µg/ml. The detection of biotin was performed by adding 100 µl of streptavidin-POD conjugate (Pierce) diluted 1:8000 in washing solution. After washing, the plate wells were incubated with 100 µl of BM blue POD substrate (Roche, Germany) in the dark at room temperature for 10 min. Then, the reaction was stopped by adding 50 µl of 0.8 M H_2SO_4. The optical density (OD) was measured at 450/540 nm on a plate reader (TECAN).

3 Results and Discussion

Most of the data presented in this dissertation are published, and summarized herein. Unpublished data are described in detail.

3.1 Role of meprin α and meprin β in collagen assembly in skin

Application of the proteomic analyses TAILS in a cell culture system revealed cleavage in procollagen α2(I) by both meprin α and meprin β [10]. This cleavage would lead to the removal of the C-propeptide of the α2 chain of type I procollagen implicating the role of meprins in collagen fibril formation. Additionally, it has been shown recently that both, meprin α and meprin β cleave off the C-propeptides from fibrillar procollagen III *in vitro* at exactly the same site and even more efficient than the procollagen C-proteinase BMP-1 [37].

To investigate the procollagen proteinase activity of meprin α and meprin β *in vitro*, human recombinant procollagen I heterotrimer consisting of two α1(I) and one α2(I) molecules was used as substrate (Fig. 5A). Procollagen was incubated with meprin α or meprin β for 1, 10, 30, and 90 minutes and processing was analyzed by Western blotting with specific antibodies raised against the procollagen α1(I) C-propeptide, N-propeptide or C-telopeptide. As a control, procollagen I was also processed with recombinant BMP-1 in the presence of procollagen C-proteinase enhancer (PCPE) -1, which is known to stimulate BMP-1 proteinase activity on fibrillar procollagen [34]. As expected, BMP-1 generated pN-collagen by removing the C-propeptides but not the N-propeptides, corresponding to its PCP activity (Fig. 5B). Interestingly, in the presence of meprin α as well as of meprin β not only the C-propeptides but also the N-propeptides were cleaved off from procollagen I, leading to the release of mature collagen I (Fig. 5B). Obviously, the maturation process of

procollagen I, induced by meprin β was more efficient compared to meprin α, resulting in full conversion of procollagen I already after 30 minutes. [40].

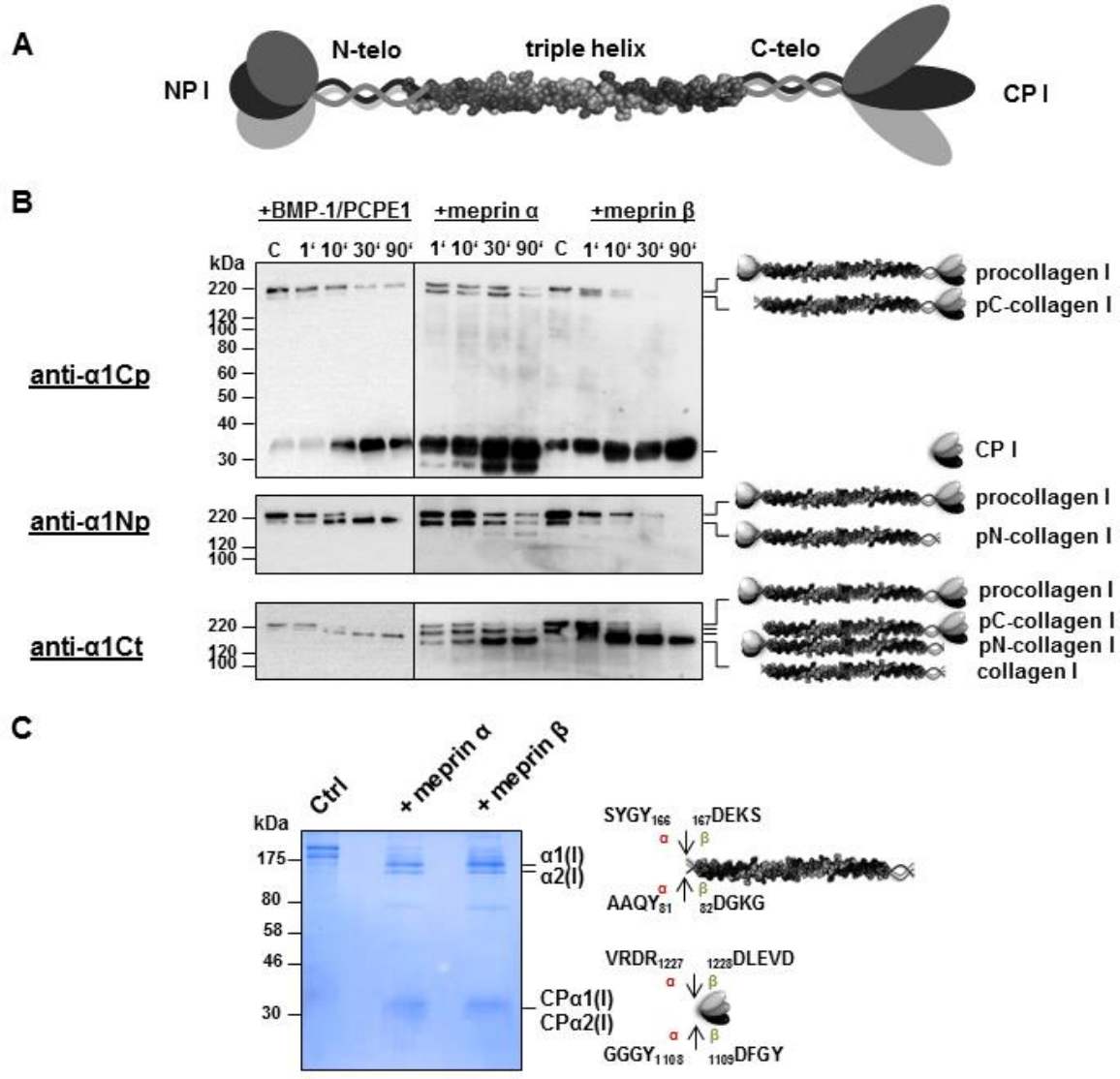

Figure 5: Cleavage of type I procollagen by meprin α and meprin β.

(A) Schematic of the type I procollagen molecule consisting of an N-terminal propeptide (NP I), the N-telopeptide (N-telo), the triple helical region, the C-telopeptide (C-telo) and the C-terminal propeptide (CP I). (B) Cleavage of recombinant procollagen heterotrimer by BMP-1, meprin α, and meprin β after 1, 10, 30, and 90 min. Processing analyzed by SDS-PAGE (10% w/v polyacrylamide) under reducing conditions followed by Western blotting using anti-collagen α1(I) C-propeptide antibody (anti-α1Cp), anti-collagen α1(I) N-propeptide antibody (anti-α1Np), and anti-collagen α1(I) C-telopeptide antibody (anti-α1Ct). Magic Mark XP (Invitrogen) was used as molecular weight marker. (D) Cleavage of procollagen I for proteomics analysis. Arrows indicate cleavage sites analyzed by proteomics for meprin α (α) and meprin β (β). Numbers display positions of amino acids in the full-length protein [40].

In order to identify the cleavage sites in procollagen I generated by meprin α or meprin β LC-MS based proteomics analyses were performed. Cleavage by meprin α and meprin β occurred at position Ala1218/Asp1219 in full-length procollagen α1(I) (Fig. 5C). Additionally, analyses of the released C-propeptides revealed cleavage at positions Arg1227/Asp1228 and Tyr1108/Asp1109 in the procollagen α1(I) and α2(I) chains, respectively (Fig. 5C). Further meprin α and meprin β cleavage sites in the N-propeptides of the procollagen α1(I) and α2(I) chains were identified at positions Tyr166/Asp167 or Tyr81/Asp82, respectively (Fig. 5C) [40].

The removal of the globular N- and C-propeptides is the key step in the formation of the collagen fibril. After enzymatic cleavage of the propeptides mature collagen monomers spontaneously assemble into collagen fibrils with the characteristic D-banding pattern [45,46]. Although not all identified cleavage sites in procollagen I were identical with the known cleavage sites for BMP-1 and ADAMTS-2, *de novo* collagen fibril formation visualized by electron microscopy could be observed only in the presence of meprin α or meprin β. As expected, BMP-1 was not able to trigger self-assembly of collagen fibrils, as this protease removed the C-propeptides but not the N-propeptides of procollagen I (Fig. 5, 6). In contrast, meprin α and meprin β induced self-assembly of collagen fibrils, consistent with their procollagen C- and N-proteinase activity (Fig. 5B, 5C). Particularly meprin β was able to trigger the characteristic D-banding pattern, due to its more efficient removal of the propeptides as deduced from Western blot analysis (Fig. 5B, 6A) [40]. Thus, meprin α and meprin β are the first known procollagen proteinases which are able to remove both the C- and the N-propeptides from procollagen I thereby inducing collagen fibril formation *in vitro*.

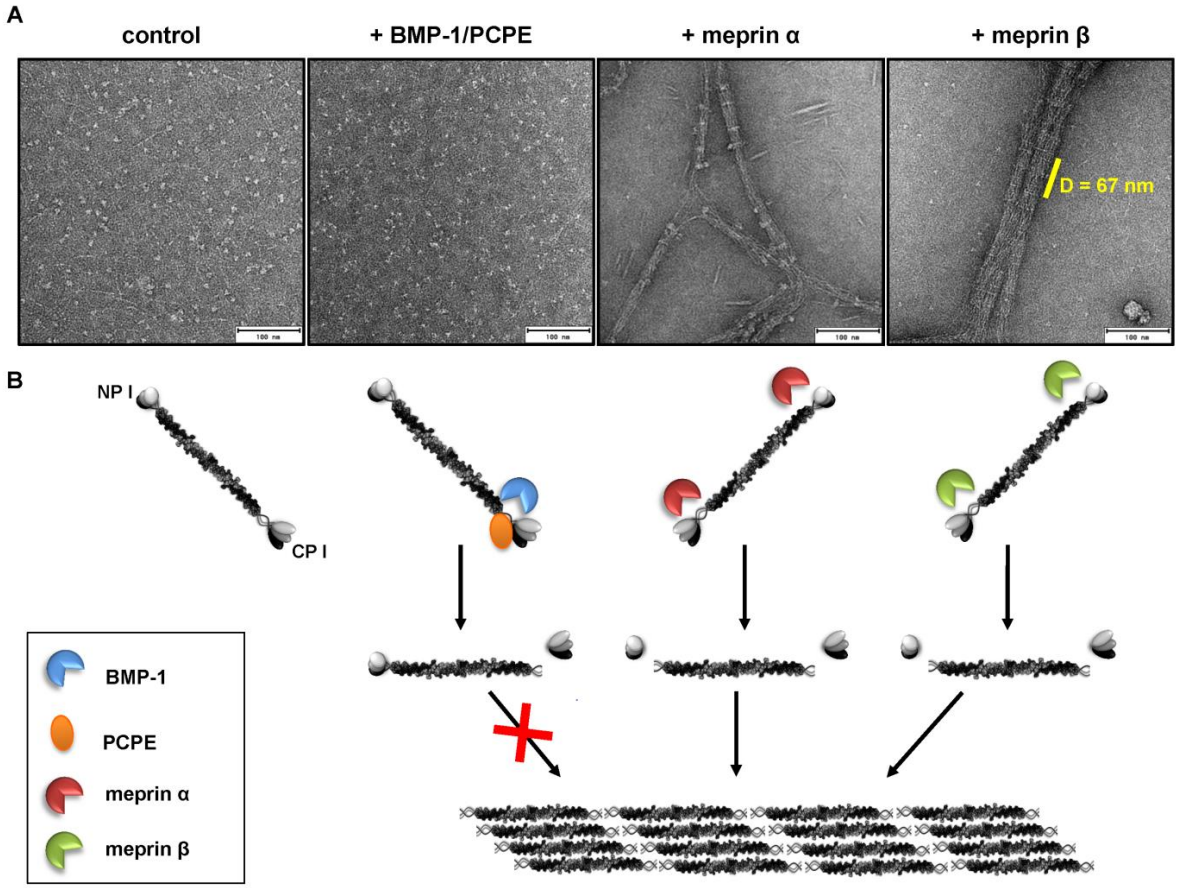

Figure 6: *De novo* fibrillogenesis of type I collagen after cleavage by meprins.

(A) Transmission electron micrographs of negatively stained collagen fibrils assembled after cleavage of recombinant procollagen type I heterotrimer by meprin α and meprin β after 60 min. As a control, untreated recombinant procollagen I was visualized. (B) Cartoon summarizes procollagen processing by different proteases and subsequent assembly of collagen fibrils [40].

In order to investigate whether meprin α and meprin β are procollagen proteinases *in vivo*, skin biopsies from wild-type, *Mep1a*$^{-/-}$, and *Mep1b*$^{-/-}$ mice were analyzed by Western blotting using antibodies against the collagen α1(I) C-propeptide or C-telopeptide. Since the anti-N-propeptide antibody did not cross-react with murine procollagen I it was not used for *in vivo* studies. Interestingly, both procollagen C- and N-proteinase activity were affected in the skin of meprin α and meprin β knockout mice (Fig. 7A, 7B). In skin lysates from meprin α and meprin β knockout mice, lower amounts of mature collagen I were observed and consequently, significantly reduced amounts of C-propeptides were detected in *Mep1a*$^{-/-}$ and

Mep1b$^{-/-}$ skin compared to the control, indicating diminished procollagen C- and N-proteinase activity *in vivo* (Fig. 7B) [40].

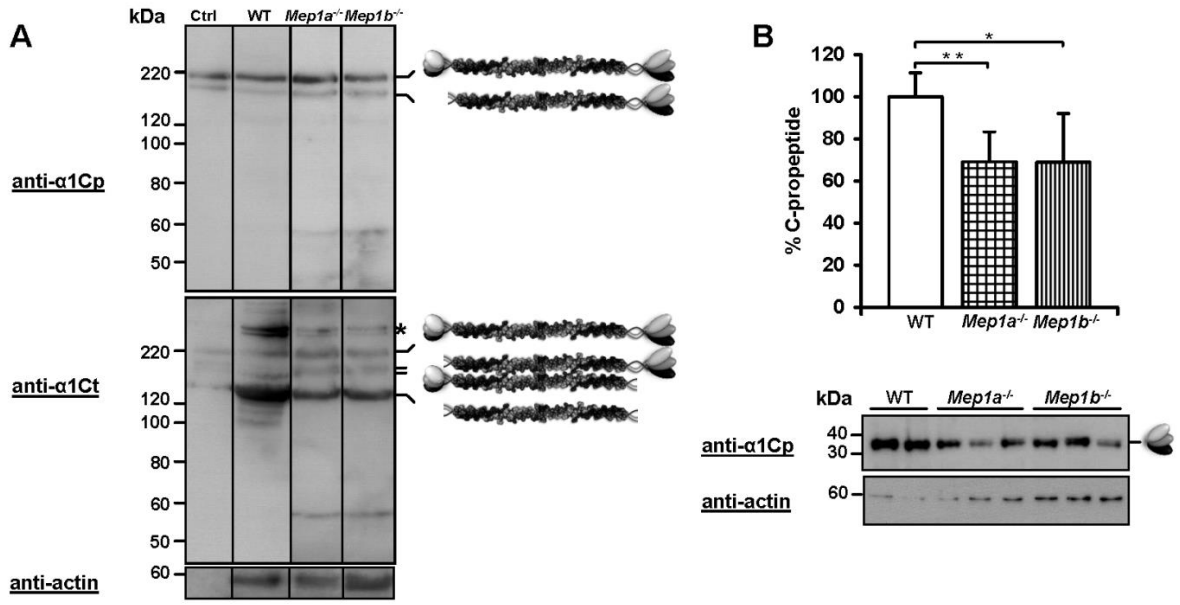

Figure 7*: In vivo* analysis of collagen I maturation in skin of WT, *Mep1a*$^{-/-}$, and *Mep1b*$^{-/-}$ mice.

Western blot analysis of skin lysates from WT, *Mep1a*$^{-/-}$, and *Mep1b*$^{-/-}$ mice (gels run in reducing conditions) using antibodies against the collagen α1(I) C-propeptide (anti-α1Cp) or C-telopeptide (anti-α1Ct) with actin as control (anti-actin) demonstrate the proteolytic processing of procollagen I *in vivo*. Asterisk indicates cross-linked mature collagen I. Ctrl: 40 nM human procollagen I heterotrimer incubated with 0.3 nM meprin α in a total volume of 50 µl, for 10 min at 37°C. (B) Western blot analyses and quantification of cleaved C-propeptides in skin lysates from WT, *Mep1a*$^{-/-}$, and *Mep1b*$^{-/-}$ mice using antibodies against the collagen α1(I) C-propeptide (anti-α1Cp) with tubulin as control (anti-tubulin). Western blots from skin lysates from each of 5 WT, *Mep1a*$^{-/-}$, and *Mep1b*$^{-/-}$ mice were quantified by using ImageJ 1.47. (*p<0.05; **p<0.01) [40].

The maturation of procollagen and the arrangement of collagen fibrils are essential for the integrity and function of connective tissue. Due to the ability of both meprins to generate mature type I collagen as well as the decreased procollagen processing observed in the skin of meprin knockout mice, the morphology and deposition of collagen fibrils was analyzed *in situ*. Histological examination of dorsal skin from *Mep1a*$^{-/-}$ and *Mep1b*$^{-/-}$ mice exhibited a significantly reduced thickness of the fibrous layer and a decreased accumulation of dermal collagen compared to

control animals (Fig. 8A, 8C), reflecting the observation of the Western blot analysis (Fig. 7). While the dermal collagen layer in wild-type mice was approximately 400 µm in thickness, in age-matched *Mep1a*$^{-/-}$ and *Mep1b*$^{-/-}$ mice corresponding thicknesses were approximately 170 µm and 150 µm, respectively (Fig. 8C) [40]. In contrast to the dramatic differences in the fibrous layer of meprin knockout and wild-type mice, no obvious morphological abnormalities in the epidermis or in the shape and number of hair follicles was observed.

Additionally, the arrangement of dermal collagen fibrils in meprin α and meprin β knockout mice was impaired compared to age-matched wild-type mice as visualized by transmission electron microscopy. While collagen fibrils in wild-type dermis displayed a compact and uniform arrangement the fibrils in *Mep1a*$^{-/-}$ and *Mep1b*$^{-/-}$ dermis were often irregularly organized, less tightly packed, and of smaller diameters compared to those in wild-type skin (Fig. 8B, 8D). A biomechanical approach revealed a significantly reduced maximum tensile strength of the skin of *Mep1a*$^{-/-}$ and *Mep1b*$^{-/-}$ mice compared to WT animals (Fig. 8E) in line with the reduced dermal collagen deposition (Fig. 8A) and the disordered organization of the collagen fibrils [40].

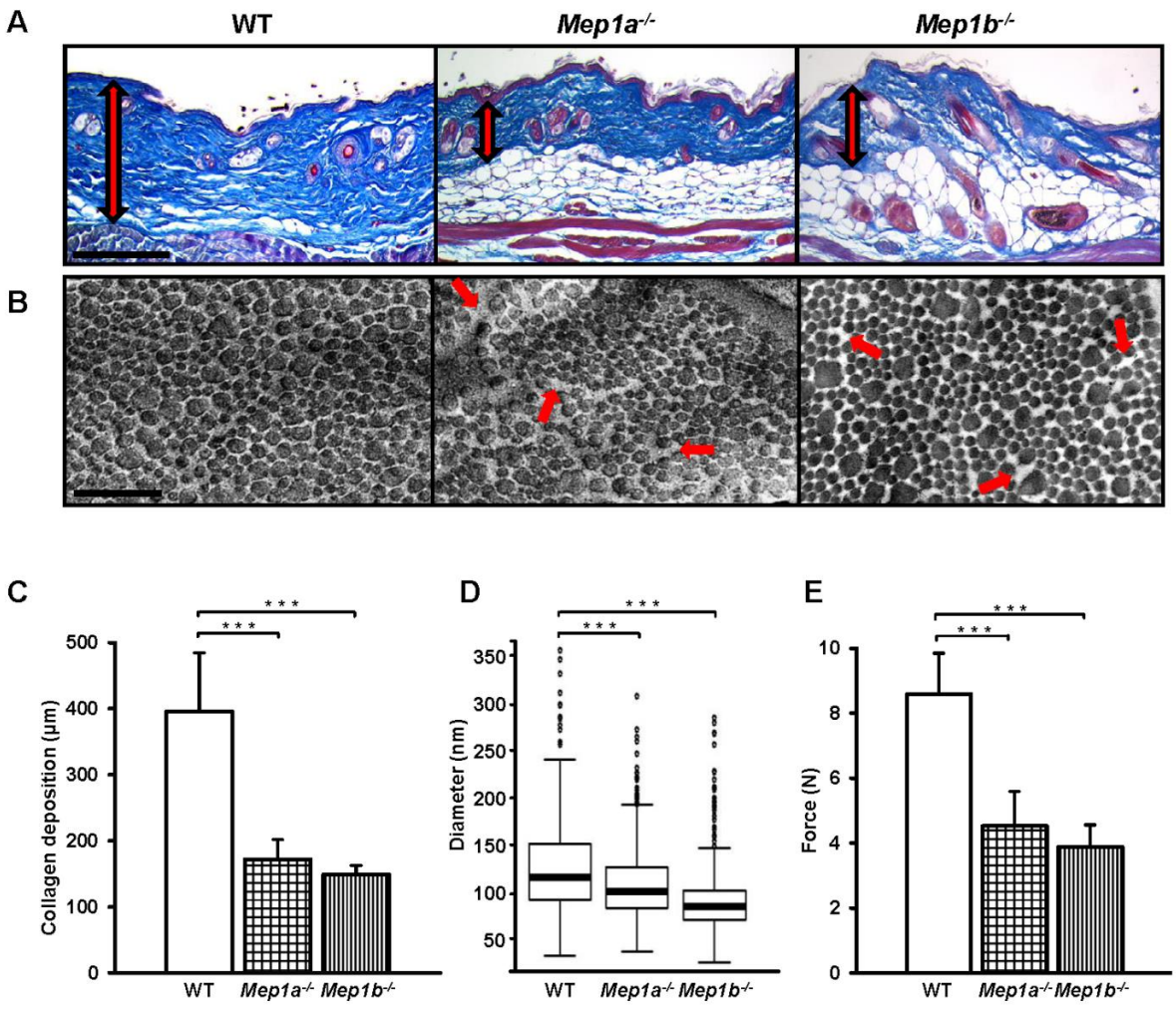

Figure 8: *In vivo* analysis of collagen I deposition and mechanical strength in skin of WT, *Mep1a*$^{-/-}$, and *Mep1b*$^{-/-}$ mice.

(A) Azan-stained skin cross-sections for visualization of collagen deposition (red arrow) in the dermis of *Mep1a*$^{-/-}$ and *Mep1b*$^{-/-}$ mice compared to the skin of age-matched wild-type animals. Scale=200 µm. (B) Dermal collagen fibrils examined by transmission electron microscopy. Fibrils in *Mep1a*$^{-/-}$ and *Mep1b*$^{-/-}$ skin cross-sections display a less tightly packed organization (red arrows) while the WT collagen fibrils show the characteristic compact and uniform arrangement. Scale bar=1 µm. (C) Dermal collagen deposition was quantified by light microscopy. The mean thickness of the different biopsies was obtained by averaging five measurements per section (***p<0.001). (D) Box plot shows the average diameters (nm) for dermal collagen fibrils of *Mep1a*$^{-/-}$, *Mep1b*$^{-/-}$, and WT mice, obtained by measuring 414 fibrils from 3 WT mice, 598 fibrils form 3 *Mep1a*$^{-/-}$ mice, and 414 fibrils from 3 *Mep1b*$^{-/-}$ mice. Bottom of the box indicates the 25th percentile, top the 75th percentile. The median values are shown as horizontal lines, indicating the 50th percentile. Whiskers indicate the lowest datum still within 1.5 interquartile range (IQR) of the lower quartile, and the highest datum still within 1.5 IQR of the upper quartile. Outliers are shown as open circles. (***p<0.001). (E) Determination of the maximum tensile strength of the skin of meprin α and meprin β knockout mice revealed a significant decrease (***p<0.001) compared to the skin of wild-type mice [40].

For many years BMP-1/tolloid-like proteinases were the only known procollagen C-proteinases *in vitro* and *in vivo*. However, in mouse embryonic fibroblasts (MEF)

isolated from *Bmp1*$^{-/-}$/*Tll1*$^{-/-}$ mice residual procollagen C-proteinase activity was present, indicating that other proteases contribute to the maturation of procollagen [36]. While Pappano et al. [36] suggested that mTLL-2 might fulfill such a role, this work provides evidence that meprin α and meprin β could be responsible for collagen I maturation *in vivo*. Interestingly, the collagen fibrils in BMP-1 deficient embryos are relatively thin in diameter and the arrangement of these fibrils is less organized compared to the wild-type control [47], which is similar to the observed phenotype in meprin α and meprin β knockout mice [40]. Recently it became obvious that astacins, including meprin α, meprin β, and tolloids, exhibit a unique family-wide cleavage specificity with negatively charged amino acid residues in P1' [38]. Consequently, this suggests most known BMP-1 substrates, like fibrillar procollagens, being candidate target molecules for meprin α and meprin β as well. In this regard, it was demonstrated that both meprins process the C-propeptide of type III procollagen *in vitro* exactly at the same site but even more efficient as BMP-1 [37]. The results of this study clearly demonstrate the physiological relevance of of meprin α and meprin β to remove the C- as well as the N-propeptide of type I procollagen, subsequently releasing fibril forming mature collagen molecules. Besides the phenotype of *Mep1a*$^{-/-}$ and *Mep1b*$^{-/-}$ mice at the histological level, the observed reduced levels of procollagen I conversion in skin of meprin knockout mice provide further evidence that meprin α and meprin β exhibit procollagen C-proteinase activity *in vivo* [40].

Previous publications demonstrated the requirement of ADAMTS-2 in the removal of the N-propeptide of type I collagen. Analogous to the procollagen C-proteinase activity of BMP-1/tolloid-like proteinases, residual procollagen N-proteinase activity was observed in ADAMTS-2 deficient mice [32]. It was proposed that ADAMTS-14 may carry out this activity, but this has not yet been demonstrated

in vivo. The present work shows, that both meprins cleave off the N-propeptides of type I procollagen *in vitro*. Additionally, reduced procollagen N-proteinase activity in skin of meprin knockout mice as well as the distinct phenotype provide strong evidence that the enzymatic activity of meprins is physiologically relevant for the removal of the N-propeptide *in vivo*. Most interestingly, identification of meprin cleavage sites by mass spectrometry revealed positions Tyr81/Asp82 in the α2 chain within an amino acid region which is known to cause Ehlers-Danlos syndrome VIIB when deleted by impaired splicing [40]. EDS VII is an inherited autosomal disorder, characterized either by an impaired splicing of exon 6, leading to the loss of the N-proteinase cleavage site and surrounding residues in the Col1A1 or Col1A2 genes [48], or by deficient ADAMTS-2 activity [49,50]. These mutations result in reduced N-terminal processing of procollagen I and subsequent disordered collagen assembly. In skin biopsies of patients with EDS VII, collagen fibrils are more loosely and randomly organized, and have smaller diameters compared to normal dermal collagen fibrils, similar to the phenotype observed in *Mep1a*$^{-/-}$ and *Mep1b*$^{-/-}$ mice [40,51]. Taken together, both meprins are involved in processing of fibrillar collagens thereby contributing to the mechanical integrity of the skin [40]. Reduced tensile strength observed in the skin of meprin α and meprin β knockout mice may result from the disorganized and thin collagen fibrils, and a diminished dermal collagen deposition as a product of decreased collagen maturation [40].

Nevertheless, the fact that *Mep1a*$^{-/-}$ and *Mep1b*$^{-/-}$ mice are viable, although exhibiting ~50% reduced litters compared to WT mice [52] indicates that the loss of meprin is compensated. To investigate differential gene expression in the skin of *Mep1a*$^{-/-}$ and *Mep1b*$^{-/-}$ mice, a mouse PCR array was employed (Fig. 9A-D). Alterations in the expression of 84 genes associated with connective tissue formation were examined. Interestingly, expression of Col1a2 was about 2.5 fold increased in

Mep1a$^{-/-}$ but not *Mep1b*$^{-/-}$ mice, whereas Col3a1 was slightly decreased in the skin of meprin α and meprin β knockout animals (Fig. 9A, 9B). However, the overexpression of Col1a2 in *Mep1a*$^{-/-}$ mice did not compensate the reduced collagen deposition in skin of these mice. Fibrillar collagen degrading enzymes, including the interstitial and neutrophil collagenases Mmp1a, 2, 3, 8, 9, 13, and 14, showed a general tendency of decreased gene expression (Fig. 9A, 9C). The same was observed for Timp1 and 3 (tissue inhibitors of metalloproteases), whereas Timp2 and 4 were significantly increased in *Mep1a*$^{-/-}$ but not *Mep1b*$^{-/-}$ mice (Fig. 9A, 9D) [40]. TIMP-3 is known to inhibit the N-proteinase ADAMTS-2 [53]. A decrease in Timp3 expression would consequently lead to an increase in procollagen N-proteinase activity of ADAMTS-2 in meprin knockout mice. However, the regulation at the mRNA level is insufficient to compensate the loss of the N-proteinase activity of meprin in skin of meprin knockout mice, indicating once again the implication of meprins in procollagen processing *in vivo.*

Since procollagen C-proteinase activity is associated with the BMP-1/tolloid-like proteinases, that is BMP-1 itself and its splice variant mammalian tolloid (mTLD), which were not included in the fibrosis PCR array, the expression of these enzymes was analyzed in the absence of meprin α or meprin β by quantitative real-time PCR. In *Mep1a*$^{-/-}$ and *Mep1b*$^{-/-}$ skin, and also in corresponding primary fibroblasts, the mRNA expression of BMP-1/mTLD was significantly increased compared to the wild-type control (Fig. 9E, 9F). In the skin of knockout animals a 2-fold increase of BMP-1/mTLD expression was observed, which was lower in the *Mep1a*$^{-/-}$ fibroblasts, but still significant. Although, BMP-1 and mTld are overexpressed in meprin deficient animals and may partially compensate the loss of procollagen C-proteinase activity, this is apparently insufficient to maintain the full conversion of procollagen into physiologically required amounts of fibril forming molecules [40].

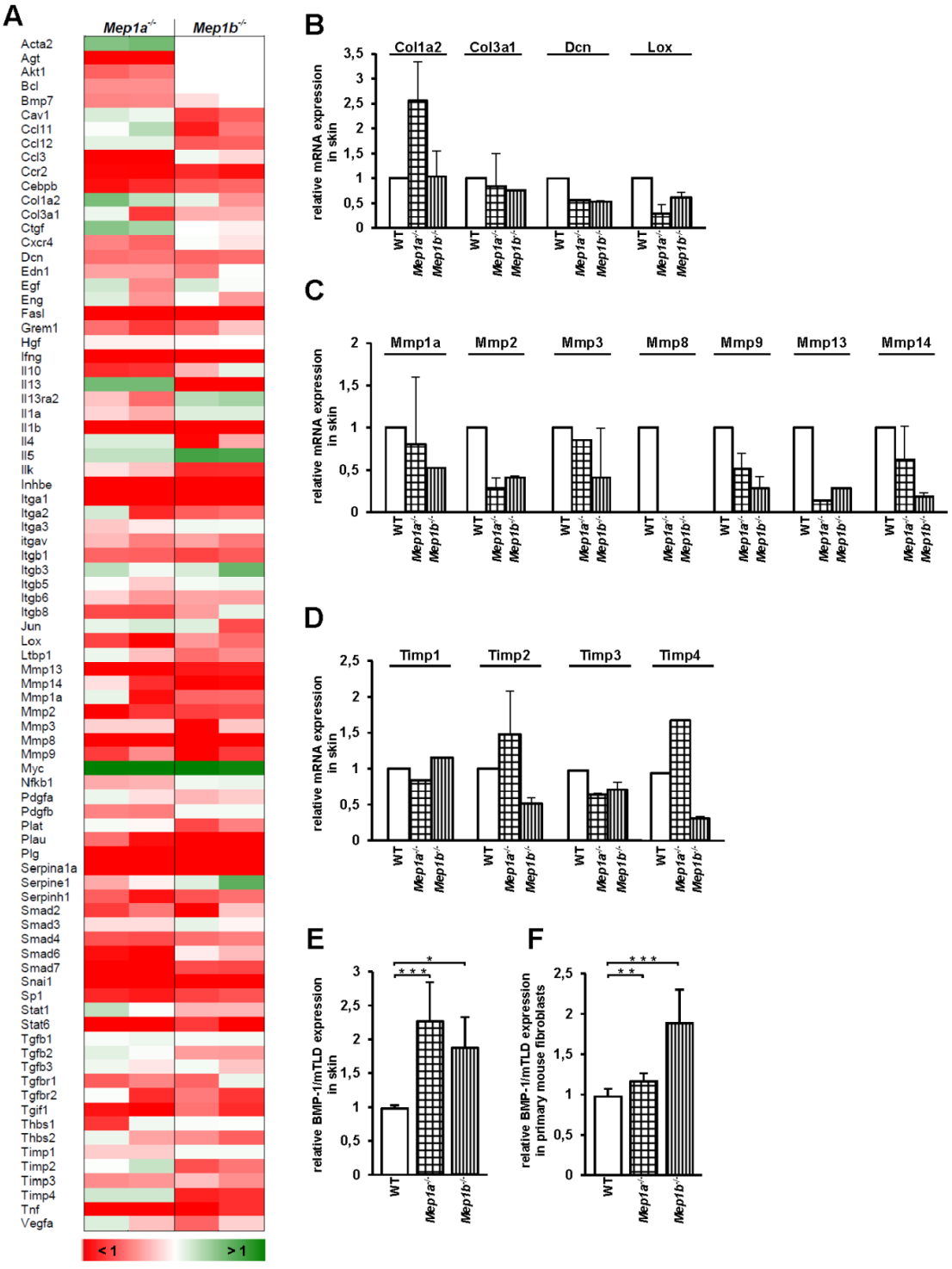

Figure 9: Regulation of fibrosis relevant genes in skin of *Mep1a*$^{-/-}$ and *Mep1b*$^{-/-}$ mice.

(A-D) 84 genes were quantified in duplicates from two different animals of each genotype using a mouse fibrosis PCR array. (A) The color code indicates the extent of change between knockout and wild-type mice (set as 1.0). (B-D) Relative expression of genes relevant for collagen assembly is shown in detail. Relative expression of BMP-1/mTLD mRNA in the skin of *Mep1a*$^{-/-}$ and *Mep1b*$^{-/-}$ mice (E) and in corresponding primary fibroblasts (F) was analyzed by quantitative real-time PCR. (*p<0.05); **p<0.01; ***p<0.001). Error bars show SD, n=3 [40].

MMPs play a key role in ECM remodeling and exhibit proteolytic activity against mature type I collagens [54]. In the mass spectrometry based approach TAILS, which enables the identification of native protein substrates *in cellulo*, MMP-1 was identified as a substrate for meprin α and meprin β revealing a cleavage site within the catalytic domain (Fig. 10A, 10B). Since an intact active site is essential for the catalytic activity of MMP-1, it was of interest to analyze whether cleavage by meprins directly affects the collagenolytic activity of MMP-1. MMP-1 is secreted as a zymogen and requires the removal of its propeptide [55]. The prodomain was displaced from the active site by treatment with p-aminophenylmercuric acetate (APMA). Differences in the collagenase activity of MMP-1 cleaved by meprin α and meprin β compared to the unprocessed enzyme were investigated by activity assays (Fig. 10C). When proMMP-1 was first incubated with meprin α or meprin β and subsequently activated with APMA, the collagenase activity decreased to 27% and 43%, respectively, compared to untreated active MMP-1. Even lower collagenolytic activity of about 13% was measured when active MMP-1 was processed by meprin α or meprin β (Fig. 10C) [40]. Hence, the collagenolytic activity of MMP-1 might be increased in the absence of meprin α and meprin β, resulting in reduced collagen deposition in skin of meprin α and meprin knockout mice.

A

peptide identified	meprin α vs. ctrl	meprin β vs. ctrl	cleavage site
DAHFDEDER	35.00	17.91	GIGG(193).(194)DAHF

B

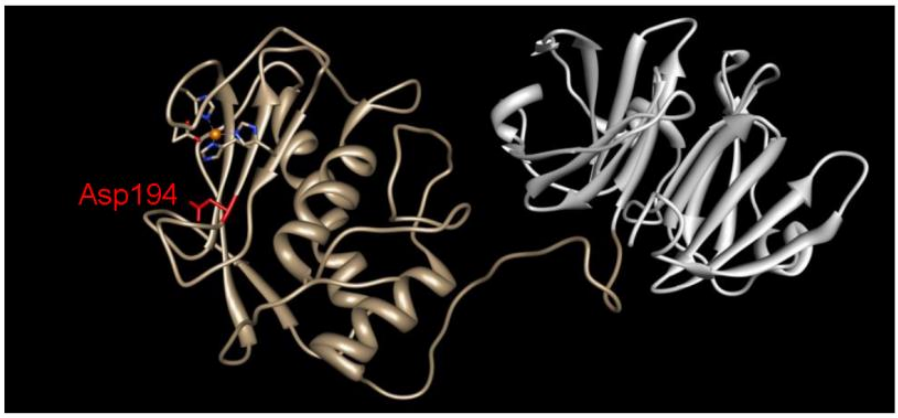

C

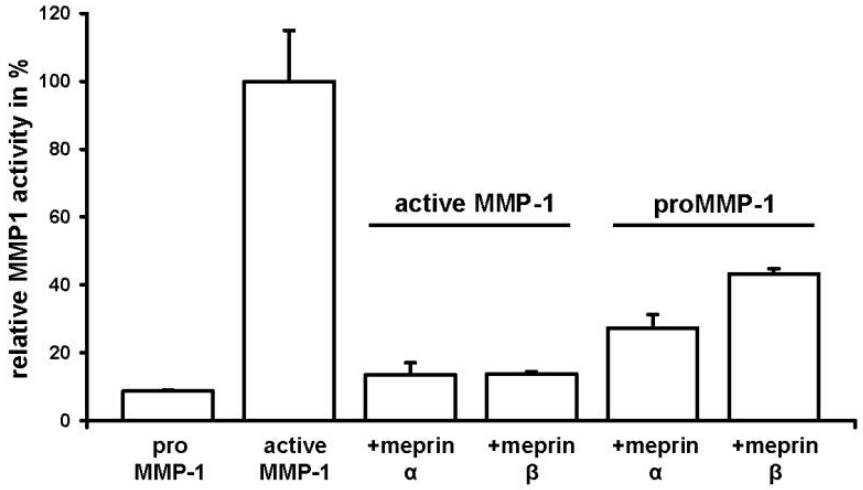

Figure 10: Influence of meprin α and meprin β on the collagenolytic activity of MMP-1.

(A) Meprin cleavage site in MMP-1 identified by TAILS [10]. Probability values were calculated by the iProphet algorithm, with high confidence in spectrum to peptide assignments. Meprin α or meprin β treated cells vs. control cells (ctrl) abundance ratios of >15 identify meprin generated neo-N-termini as high confidence cleavage products. Sequences are given in one letter code. For detailed information see [10]. (B) Crystal structure of MMP-1 (pdb 2CLT) with the meprin cleavage site (Asp194 in P1') identified by TAILS highlighted in red. The catalytic domain of MMP-1 is show in brown and the hemopexin domain in grey. The catalytic zinc in the active site cleft is displayed in orange, complexed by three histidines (blue) and one aspartate residue (red). Image produced using the UCSF Chimera package from the Resource for Biocomputing, Visualization, and Informatics at the University of California, San Francisco (supported by NIH P41 RR-01081)[56]. (C) Relative activity of MMP-1 with or without meprin α or meprin β was determined using the fluorogenic peptide MOCAc-Pro-Leu-Gly-Leu-A2(Dnp)-Ala-Arg-NH_2. Proteolytic activity was calculated relative to the emission at 405 nm with an excitation at 320 nm [40].

3.2 Meprin α and meprin β modulate the release of procollagen from Hsp47 *in vitro*

The proper assembly of the procollagen I molecules during the transport across the Golgi apparatus to the extracellular space is mainly regulated by the procollagen-binding protein Hsp47 [43]. Interestingly, the proteomics approach TAILS revealed two cleavage sites within Hsp47 for meprin α as well as meprin β (Fig. 11A) [10]. Incubation of Hsp47 with meprin α or meprin β at pH 7.5 induced a time dependent processing of Hsp47 after 30 min (Fig. 11B). However, this processing was limited at pH 7.5 and it could be improved at lower pH conditions, leading to a full conversion of the full-length Hsp47 by meprin β into the processed form (Fig. 11B).

To investigate, whether the cleavage of Hsp47 by meprin α and meprin β has any effect on the interaction between procollagen and Hsp47, a specific collagen binding ELISA was performed. Collagen I was coated on 96-well plates and incubated with native or cleaved Hsp47. Indeed, when cleaved by meprin α or meprin β, the collagen binding affinity of Hsp47 was up to 5 fold decreased (Fig. 11C). This reduction in collagen binding of Hsp47 could be decreased by addition of actinonin, a specific meprin α and meprin β inhibitor. Thus, the dissociation of procollagen from Hsp47 might be a meprin dependent process *in vitro*.

A

peptide identified	meprin α vs. ctrl	meprin β vs. ctrl	cleavage site
DEEVHAGLGELLR	35.00	35.00	SAEQLR(103).(104)DEEVH
EWAAQTTDGK	24.33	35.00	ALQSIN(174).(175)EWAAQT

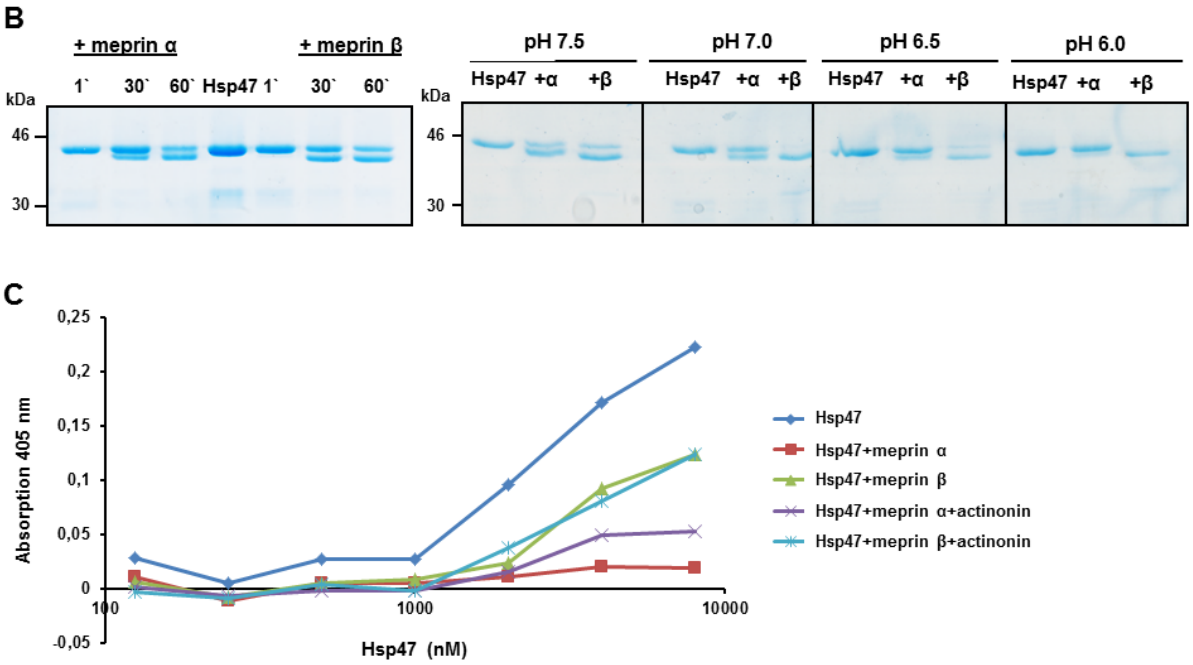

Figure 11: Meprin α and meprin β cleave Hsp47 and reduce its collagen binding affinity *in vitro*.

(A) Meprin cleavage site in Hsp47 identified by TAILS [10]. Probability values were calculated by the iProphet algorithm, with high confidence in spectrum to peptide assignments. Meprin α or meprin β treated cells vs. control cells (ctrl) abundance ratios of >15 identify meprin generated neo-N-termini as high confidence cleavage products. Sequences are given in one letter code. [10]. (B) Time and pH depended processing of recombinant Hsp47 by meprin α and meprin β. 5 µg Hsp47 were incubated with 15 nM recombinant meprin α or meprin β, in a total volume of 10 µl for 1, 30, and 60 minutes at 37°C, in 20 mM HEPES at pH 7.5, 7.0, 6.5 or 6.0. Proteins were separated by SDS-PAGE under reducing conditions and subsequently stained with coomassie. (C) For collagen-binding ELISA rat tail collagen was coated on 96-well plates and incubated with the indicated concentration of recombinant Hsp47 which was prior processed with 15 nM human recombinant meprin α or meprin β in the presence or absence of 10 µM actinonin. Binding was detected as described in [43].

3.3 Meprin α and meprin β are potential therapeutic targets to limit fibrosis

The regulation of ECM remodeling depends on complex molecular interactions and is therefore a key event in many physiological conditions. A tight balance between the synthesis and breakdown of ECM is required for the function of all tissues and leads, when dysregulated, to pathophysiological events, such as arthritis,

cancer, atherosclerosis, aneurysm and fibrosis [57,58,59,60,61,62,63]. In fibrotic skin tissues, such as hypertrophic scars or keloids, an increased synthesis and deposition of collagen is observed [64]. However, it is not clearly understood whether the excessive accumulations of collagen in fibrotic tissues are due to uncontrolled procollagen synthesis, maturation or reduced collagen degradation.

This work demonstrates that meprin α and meprin β are involved in posttranslational modifications of collagens at different levels, as by inducing of the release of procollagen from Hsp47 during the secretory pathway, by enzymatic conversion of procollagen into fibril forming molecules, and by regulating the activity of the collagen degrading enzyme MMP-1. Recently, Kronenberg et al. showed that in the dermis of human keloids, both meprin α and meprin β are overexpressed [37]. Thus, inhibition of meprins in skin could offer a promising approach for the regulation of meprin mediated collagen deposition in fibrotic skin.

The initial idea for the development of specific meprin α and meprin β inhibitors was raised by the finding that meprin β as well as meprin α have a striking preference for negatively charged residues at the P1' position (Fig. 12A) [38]. This cleavage specificity was also found to be characteristic for other astacin proteases as the procollagen C-proteinase BMP-1. Apart from astacin proteases, no other extracellular proteases share this particular substrate motif, suggesting that many cleavage events seen *in vivo* exhibiting negatively charged amino acid residues in P1' might be due to meprin activity, or related family members [3,38]. Moreover, examination of the recently solved crystal structure of human meprin β indicated that positively charged arginine residues Arg^{516} and Arg^{567}, both part of the TRAF domain of meprin β can interact with negatively charged amino acid residues of the substrate (Fig. 12B) [3,12]. Therefore, it seems likely that small molecules resistant to proteolytic cleavage with a proper distribution of negatively charged groups might inhibit meprins.

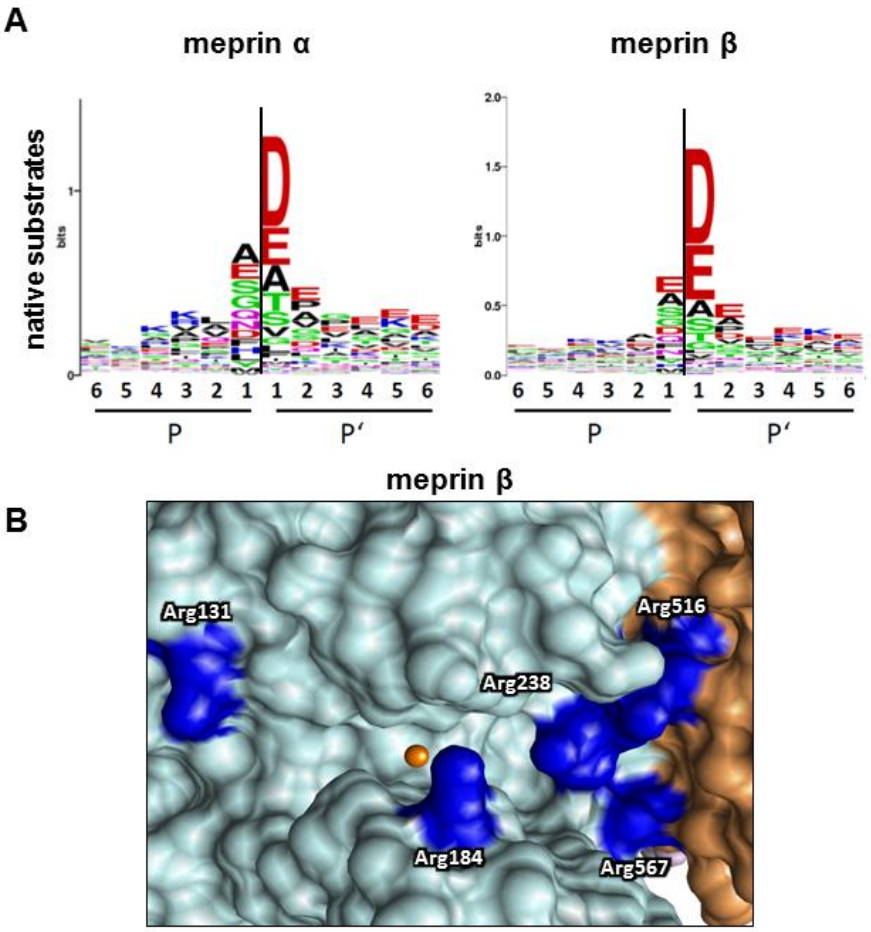

Figure 12: Cleavage specificity of meprin α and meprin β.

(A) Cleavage specificity of meprin α and meprin β displayed in the WebLogo style, where the most preferred amino acid residues are shown for positions P6 to P6'. The height of the single letter code corresponds to its occurrence. Colour-coding: acidic residues in red, basic residues in blue, polar residues (including tyrosine and glycine) in green, hydrophobic residues (including alanine and proline) in black. The black line indicates the cleavage site. WebLogo ordinates are scaled in bits as described previously [65]. Relative abundance of amino acid residues around the cleavage sites of meprin α and meprin β derived from native substrates. (B) The unique specificity of meprin β is based on structural features of the active site cleft. Positively charged arginine (Arg) residues (dark blue) can interact with negatively charged amino acid residues of the substrate. The catalytic zinc is shown in orange, the TRAF domain in brown. Numbering of amino acids is based on UniProt [3].

To explore which distribution of negatively charged groups leads to the optimal binding into the active site cleft, three different acidic quenched fluorogenic hexa-peptides P1 ((Mca)-EDEDED-(Dnp)), P2 ((Mca)-EEEEEE-(Dnp)), and P3 ((Mca)-DDDDDD-(Dnp)) were used. These three peptides were incubated with either human recombinant meprin α, meprin β or BMP-1 and the relative amount of product (*y* axis)

was calculated with regard to fluorescence intensity at 405 nm with an excitation at 320 nm, and plotted against time in seconds (*x* axis) [3]. Interestingly, only meprin β but not meprin α or BMP-1 were capable of cleaving these acidic peptides (Fig. 13). P1 containing both Asp and Glu residues was the best substrate for meprin β [3].

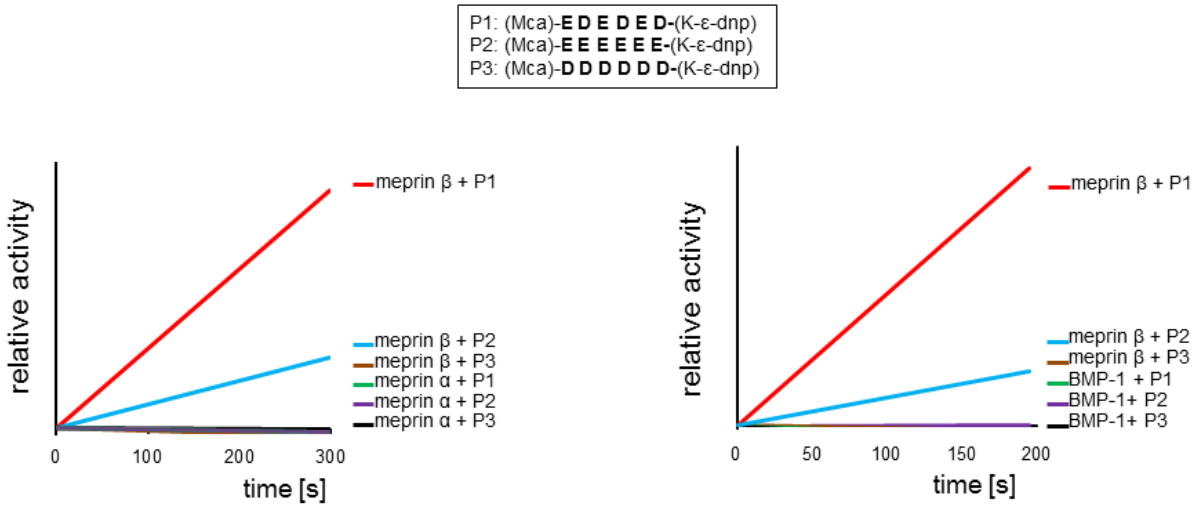

Figure 13: Meprin β cleaves completely acidic peptides.

(A) Quenched fluorogenic peptides (P1, P2, and P3) were incubated with human recombinant meprin α or meprin β or (B) BMP-1 and the relative amount of product (y axis) was calculated with regard to fluorescence intensity at 405 nm with an excitation at 320 nm, and plotted against time in seconds(x axis). Mca: (7-Methyloxycoumarin-4-yl) acetyl; dnp, 2,4-Dinitrophenyl [3].

To confirm that peptide P1 can be processed by endogenous meprin β it was applied in a cell culture based activity assay. MDCK (Madin-Darby Canine Kidney Epithelial) cells stably transfected with human meprin β or its catalytically inactive mutant E90A were used to determine the cell surface activity of meprin β. Only meprin β over-expressing cells were able to hydrolyze the acidic substrate P1 (Fig. 14A). No activity was detectable on cells overexpressing the inactive E90A mutant displaying the ability of endogenous membrane bound meprin β to cleave the Asp/Glu stretch. Thus, the application of the quenched fluorogenic peptide P1 represents a novel tool for determination and quantification meprin β surface activity in cell culture based assays.

In order to further analyze the processing of the acidic peptide by endogenous meprin β, kidney lysates were prepared form wild-type, *Mep1b*$^{-/+}$, and *Mep1b*$^{-/-}$ mice in the absence of the metalloprotease inhibitor EDTA. Only in kidney lysates from wild-type and heterozygous meprin β knockout mice activity could be detected. In kidney lysates of meprin β null mice only very low back-ground activity was detectable (Fig. 14B). This residual activity probably resulted from hydrolyzation of the peptide P1 by meprin α, since it could be inhibited in *Mep1b*$^{-/-}$ tissue lysates using actinonin (Fig. 15D). Therefore, it seems likely, that *in vivo* endogenous murine meprin α, in contrast to the human recombinant protein is able to hydrolyze the Asp/Glu stretch of the peptide P1. However, whether murine meprin α is able to cleave P1 is not clear yet and further activity assays using recombinant murine meprin α need to be performed to clarify this issue.

As deduced from the crystal structure of meprin β, the peptide P1 had the ideal distribution of negatively charged groups for the interaction with the active site cleft of meprin β and is therefore thought to be a good model for the development of an inhibitory compound. Moreover, this unique cleavage specificity of meprin β demonstrates that the application of P1 is a novel tool for the determination and quantification of meprin β activity *in vitro* and *in vivo.* Improvement of this technique might offer a method to display meprin β activity not only in tissue lysates, but also in organs of living organisms. This activity-based imaging and monitoring of meprin β activity *in vivo* would allow an accurate targeting of meprin β directly at the site of its action.

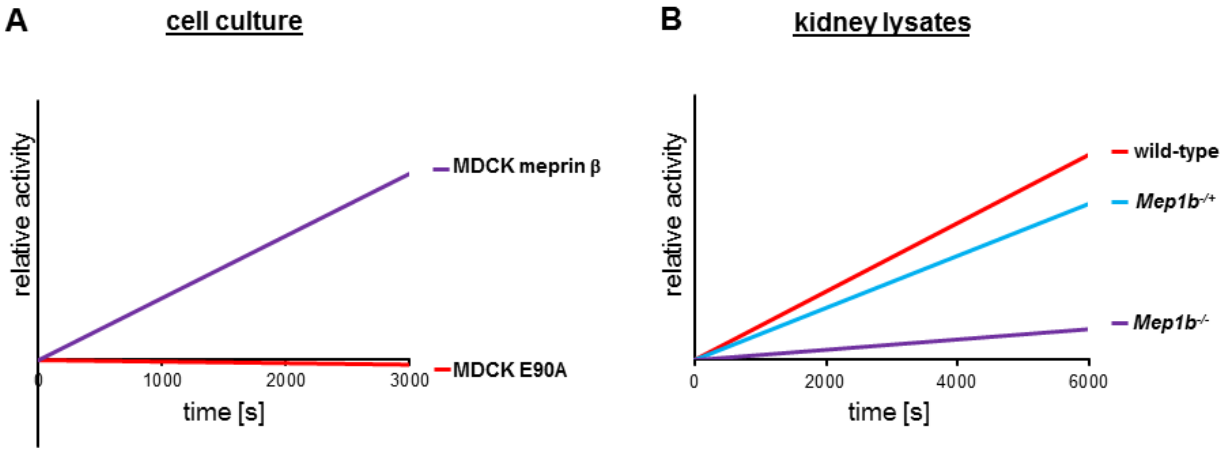

Figure 14: Endogenous meprin β cleaves acidic peptide P1 in cell culture and in kidney lysates.

(A) Cell surface activity of meprin β was analyzed using MDCK (Madin-Darby Canine Kidney Epithelial) cells stably overexpressing meprin β or the catalytically inactive mutant E90A. Equal numbers of MDCK cells were seeded in a 24-well plate and were grown until 90% confluence. Cell surface activity of meprin β was determined using quenched fluorogenic peptide P1 and the relative amount of product (y axis) was calculated with regard to fluorescence intensity at 405 nm with an excitation at 320 nm, and plotted against time in seconds (x axis). (B) Meprin activity was measured in 200 µg kidney lysate after addition of the quenched fluorogenic peptide P1.

The unique cleavage specificity and the structure of meprin β allowed the design of specific inhibitors, targeting the active site of this protease. The aim was to create a small peptide-inhibitor that is stable towards proteolysis, but still displaying the same binding properties as a substrate. This characteristic is fulfilled by phosphinic peptide-analogues where the carboxyl group of amino acids is replaced by a phosphonic mimic (Fig. 15A). Grams et al. showed, that such phosphinic peptides bind into the active site of astacin thereby mimicking the carboxy-anion of the transition state therefore being resistant to proteolytic degradation [66]. A phosphinic peptide inhibitor, which copies the structural features of the acidic peptide P1 was created by Vincent Dive (CEA, Service d'Ingénierie Moléculaire des Protéines, Cedex, France).

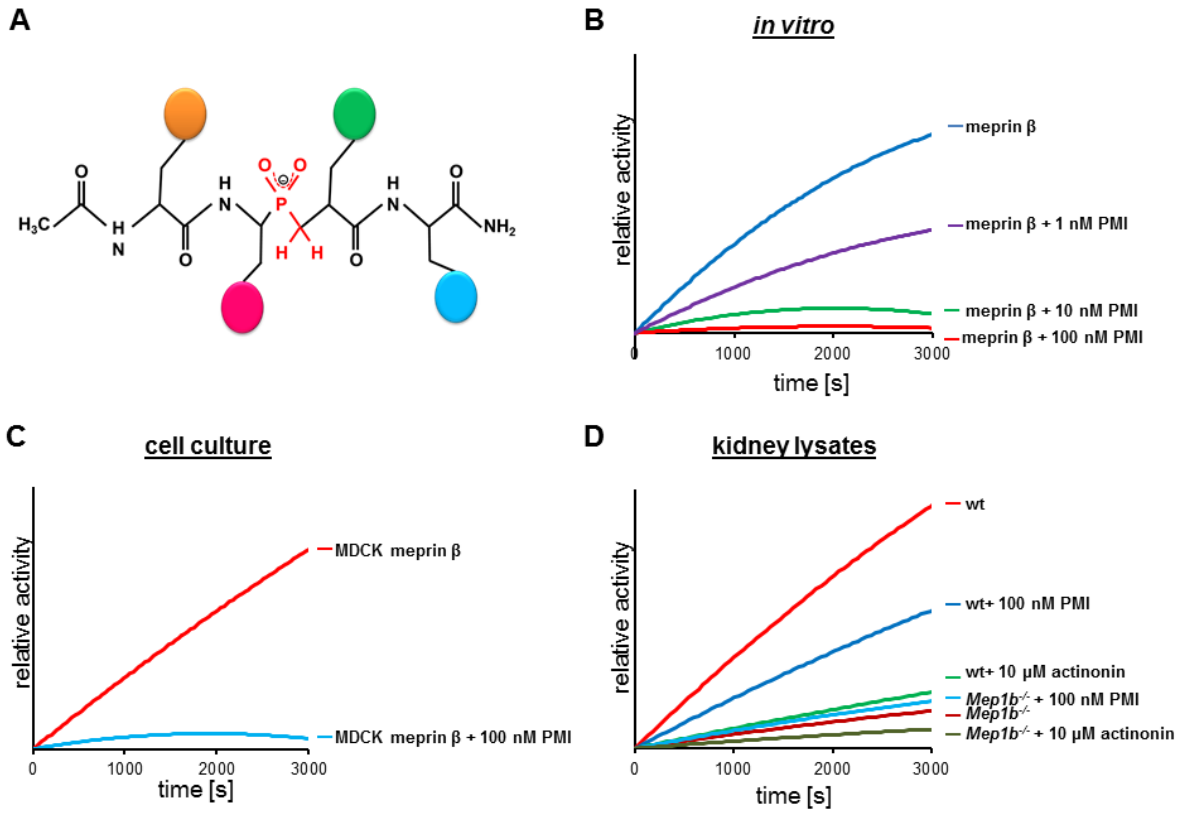

Figure 15: Phosphinic peptide inhibits recombinant and endogenous meprin β.

(A) Structure of a phosphinic peptide inhibitor. Tetrahedral phosphonic moiety is depicted in red. Orange, green, pink and blue circles indicate amino acid side chains (adapted from Vincent Dive ©CEA/V. Dive). (B) 1-100 nM phosphinic meprin β inhibitor (PMI) was incubated with active meprin β for 30 min at 37°C subsequently enzyme activity was measured using the quenched fluorogenic peptide P4. The relative amount of product (y axis) was calculated with regard to fluorescence intensity at 405 nm with an excitation at 320 nm, and plotted against time in seconds (x axis). (C) Equal amount of MDCK cells was seeded in a 24-well plate and were grown until 90% confluence. 100 nM of the inhibitor was added to 400 µl serum free cell culture medium and cell surface activity of meprin β was directly determined. (D) 100 nM phosphinic inhibitor or 10 µM actinonin were added to 200 µg kidney lysate in a total volume of 100 µl. Meprin activity was immediately measured after addition of the quenched fluorogenic peptide P1.

The phosphinic peptide inhibited human recombinant meprin β in low nanomolar concentration (Fig. 15B) and cell surface activity of human endogenous meprin β on stably transfected MDCK cells could be fully blocked with 100 nM inhibitor (Fig. 15C). The same amount of the phosphinic peptide-analogue inhibited meprin β activity in murine WT kidney lysates and showed no effect in meprin β knockout tissue, indicating the specificity of this inhibitor for endogenous meprin β *in vivo* (Fig. 15D). Interestingly, actinonin which is known to inhibit both, meprin α and meprin β induced an even stronger reduction in WT and meprin β deficient tissues

(Fig. 15D). Since the phosphinic inhibitor had a less pronounced effect on the endogenous meprin activity compared to actinonin it probably inhibited only meprin β but not meprin α in murine tissue. Moreover, the phosphinic inhibitor did not reduce the activity in meprin β deficient lysates, pointing out the specificity if this inhibitor towards endogenous meprin β.

Meprin β is implicated in many pathological processes such as inflammation, neurodegeneration, cancer and fibrosis [3]. This work demonstrates that meprins are involved in collagen deposition in skin and the absence of meprin activity consequently leads to reduced maturation and deposition of procollagen I along with an abnormal collagen fibril organization and reduced tensile strength of the skin. Moreover, meprin α and meprin β are overexpressed in dermal fibroblasts of fibrotic skin the place of collagen synthesis and maturation [37]. Therefore, it is evident that targeting meprin activity in fibrotic skin might allow for the development of a novel therapeutic approach to limit collagen deposition in this pathologic condition. Future studies using the small inhibitory mimic have to be performed to investigate its inhibitory and therapeutic potential *in cellulo* and *in vivo*. Bleomycin-induced fibrosis mouse models might help to study whether the peptide-analogue is able to inhibit meprin's procollagen C- and N-proteinase activity *in vivo* and to reduce collagen deposition in fibrotic skin.

3.4 KPI domain of APP_{751} inhibits the activity of KLK2, KLK4, and KLK7 *in vitro*

The mechanisms for regulation of a protease's activity involve endogenous activators and inhibitors. Maintenance of tightly regulated processes is crucial and the upset of this balance consequently leads to a range of pathological events, such as arthritis, cancer, atherosclerosis, aneurysms and fibrosis

[57,58,60,61,62,63,67,68,69,70,71,72]. Meprin β is secreted as a zymogen and has to be proteolytically processed by tryptic enzymes to gain activity [3]. Ohler et al. demonstrated that kallikrein-related serine peptidases (KLKs) 4, 5, and 8 are able to activate meprin β by enzymatic removal of its propeptide [5]. The activity of KLKs is mainly regulated by canonical inhibitors. The best characterized inhibitors are the Kunitz protease inhibitors (KPI) which are known to regulate the activity of a range of serine proteases, e.g. trypsin, chymotrypsin, and plasmin [73]. Interestingly, KPI can be part of larger proteins, as a functional module within a multi-domain molecule [74]. This is the case for the amyloid precursor protein (APP) isoform 751 which possesses a KPI-domain (Fig. 16A) [75]. Recently, it was demonstrated that meprin β exhibits β-secretase activity, thereby releasing the soluble ectodomain of APP into the extracellular space [14]. On the other hand, meprin β activates the α-secretase ADAM10, which also sheds APP from the cell surface [10]. Therefore, it was of great interest to analyze whether soluble APP_{751} ($sAPP_{751}$), containing a functional KPI domain is able to inhibit KLKs, consequently regulating the activation of promeprin β.

Indeed, $sAPP_{751}$ was able to inhibit KLK2, 4 and 7 in the same manner as the recombinant KPI domain (Fig. 16B, 16C). Recombinant $sAPP_{751}$ inhibited the activity of KLK2 and KLK4 down to 20-30%, while the KPI domain alone reduced the activity of KLK2 and KLK4 down to 30-40% (Fig. 16B, 16C). After incubation with the recombinant KPI domain, KLK7 exhibited only about 40% residual activity. Interestingly, no KLK 7 activity could be detected in the presence of $sAPP_{751}$ (Fig. 16B, 16C). Inhibition kinetics were determined to analyze affinity of the $sAPP_{751}$ towards the KLKs, revealing an IC_{50} of 9.55 nM, 74.32 nM, and 3.695 nM for KLK2, KLK4, and KLK7, respectively.

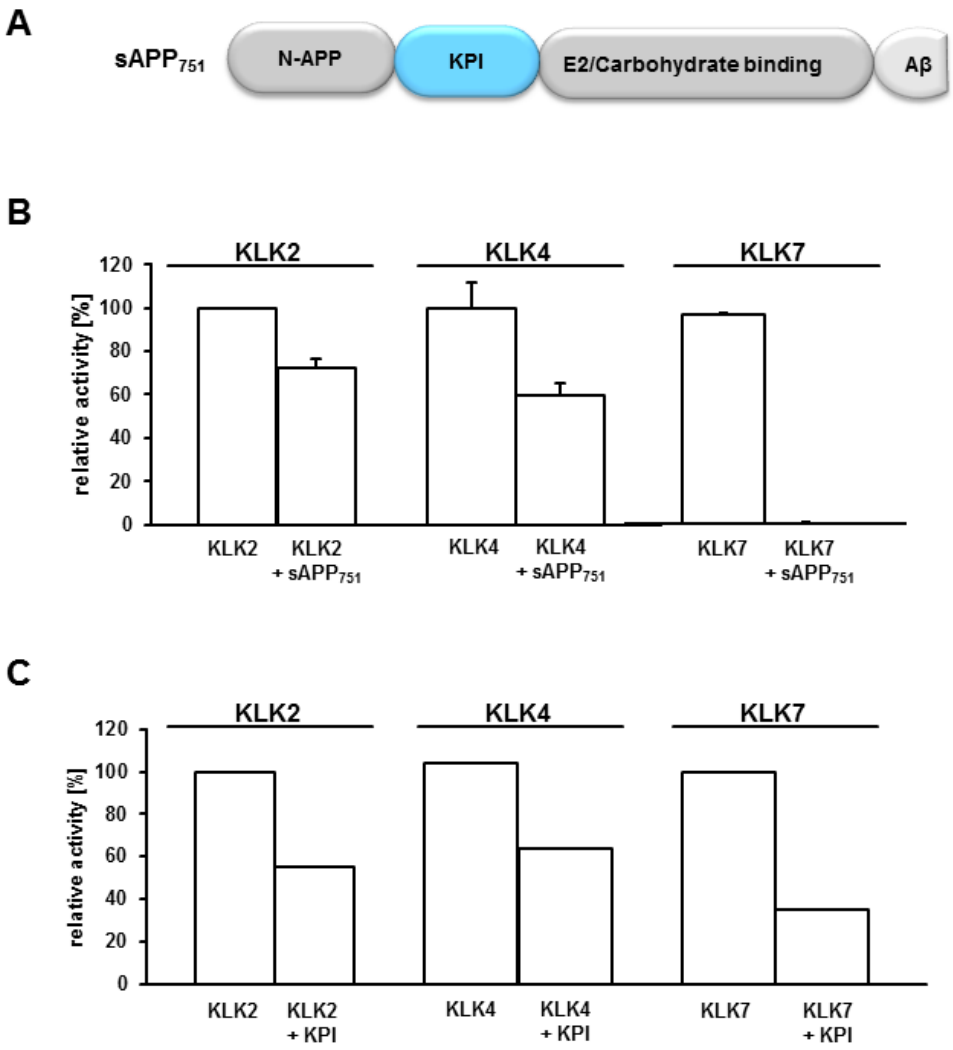

Figure 16: $sAPP_{751}$ and the KPI domain inhibit the activity of KLK2, KLK4, and KLK7 *in vitro*.

(A) The soluble ectodomain of APP_{751} contains a N-terminal domain (N-APP), followed by the KPI domain, E2/carbohydrate binding domain and a truncated Aβ domain. (B) Recombinant $sAPP_{751}$ and (C) the KPI domain alone (kind gift from Prof. Dr. Axel J. Scheidig, Institute of Zoology, Christian-Albrechts-University, Kiel) were incubated with recombinant KLK2, 4 and 7 for 10 min at 37°C in 50 mM Tris/HCl buffer, pH 8.0, containing 100 mM NaCl and 0.005% Tween 20. All activity assays were performed in duplicates in a 96-well plate in a total volume of 100 µl. Activity of KLK2 and KLK4 was determined using the quenched fluorogenic peptide Z-Pyr-Gly-Arg-Mca. For KLK7 activity measurements the quenched fluorogenic peptide Suc-Leu-Leu-Val-Tyr-AMC was applied.

Kunitz serine protease inhibitors are characterized by their resistance to proteolysis through a disulfide-stabilized double loop structure. The KPI is able to bind the active site of the target enzymes in a substrate-like manner, since the reactive peptide bond is orientated ideally for proteolytic cleavage [76]. However, this noncovalent complex consisting of 3 disulfide bonds persists being resistant to

proteolysis. The KPI domain is often expressed as a functional module within a multi-domain protein such as APP_{751}.

Full-length APP_{751} is a transmembrane protein which is expressed in the basal layer of epidermis where it fulfills a variety of distinct biological roles [77,78]. sAPPα, generated by the metalloprotease ADAM10, has been demonstrated to be a potent epidermal growth factor due to its mitogenic activity [77]. Interestingly, meprin β has previously been shown to activate ADAM10 through cleavage of the propeptide [10]. When active, ADAM10 releases sAPPα that might than interact with other soluble serine proteases such as KLK2, KLK4, and KLK7 thereby regulating their activity within this proteolytic web (Fig. 3, 17). Additionally, meprin β itself is able to act as β-secretase, also being able to release the ectodomain of APP into the extracellular space [14]. Ohler et al. postulated, that in skin KLK4 activates meprin β by proteolytic removal of its propeptide [5]. Once activated, meprin β induces terminal differentiation of keratinocytes in skin [22]. Thus, when inhibited through $sAPP_{751}$, KLK4 is not able to cleave off the propeptide of promeprin β and promeprin β remains in its inactive state, unable to induce APP ectodomain shedding. This negative feedback loop might be relevant for the regulating of the cell cycle and differentiation of keratinocytes where both proteases meprin β and ADAM10 seem to be important players. However, this has to be studied in detail in cell culture based assays and investigations have to be performed to understand the effect of meprin mediated sAPP release within the proteolytic web. For instance, mass spectrometry analyses of the secretome of APP knockdown keratinocytes could help to understand the regulatory role of sAPP in skin. Moreover, in addition to meprin β induced ectodomain shedding of APP, meprin β processes APP at the N-terminus, generating N-APP fragments. Whether this cleavage has any effects on the inhibitory capacity of $sAPP_{751}$ has to be elucidated in further inhibition studies.

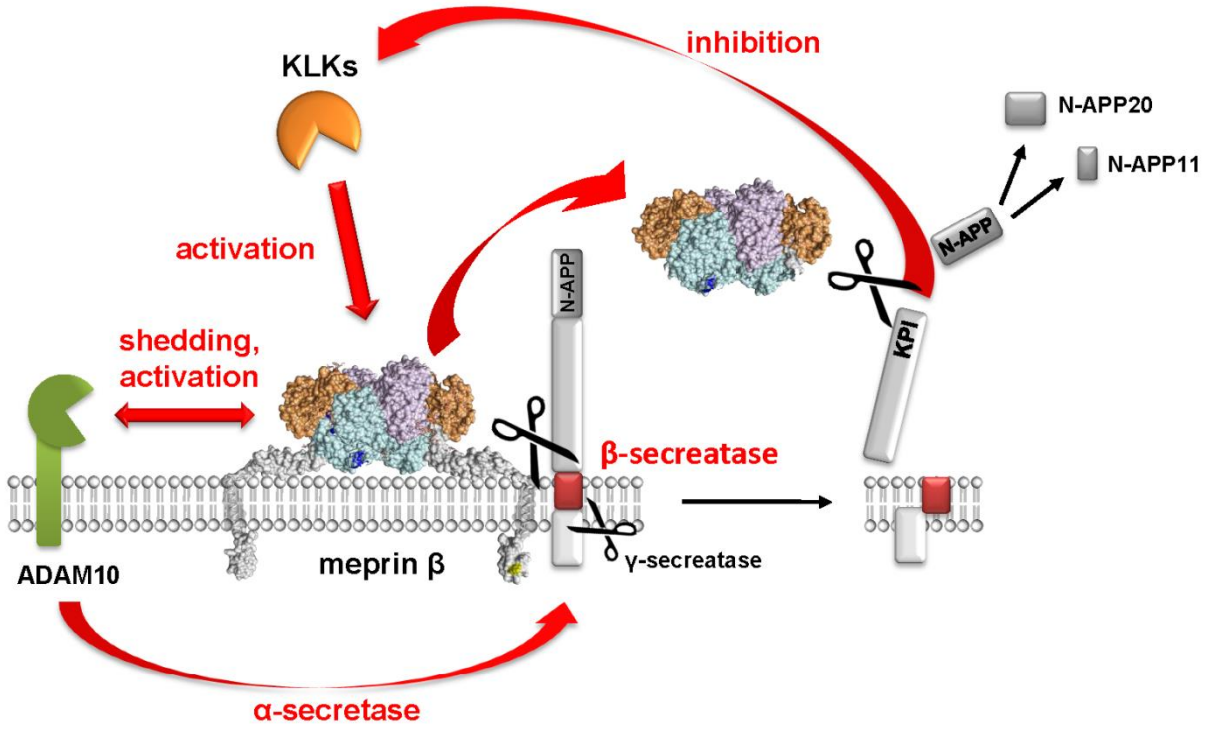

Figure 17: Negative feedback regulation of meprin β activity within the proteolytic web.

Promeprin β can be activated by human tissue KLKs. When active, membrane-bound meprin β generates soluble APP which in turn affects the activity of KLKs. On the other hand meprin β activates the constitutive α-secretase ADAM10 [10] which performs ectodomain shedding of APP, thereby indirectly regulating meprin β activity.

3.5 Development of a specific sandwich ELISA for detection of meprin α

In order to generate monoclonal antibodies (mAb) against meprin α, BALB/c mice were immunized with human recombinant promeprin α with a N-terminal Strep-tag as previously described [44]. Supernatants of hybridoma cells were tested for production of anti-meprin α mAb by ELISA. Eighteen positive clones were obtained (M41-1 to M41-18) and tested for antigen recognition by Western blotting. Western blot analyses revealed that all generated mAb were able to recognize recombinant meprin α (Fig. 18). Interestingly, anti-meprin α mAbs M41-1, M41-3, and M41-5 were able to bind an epitope within the pro-domain of meprin α, thereby recognizing only the recombinant promeprin α (Fig. 18, 19).

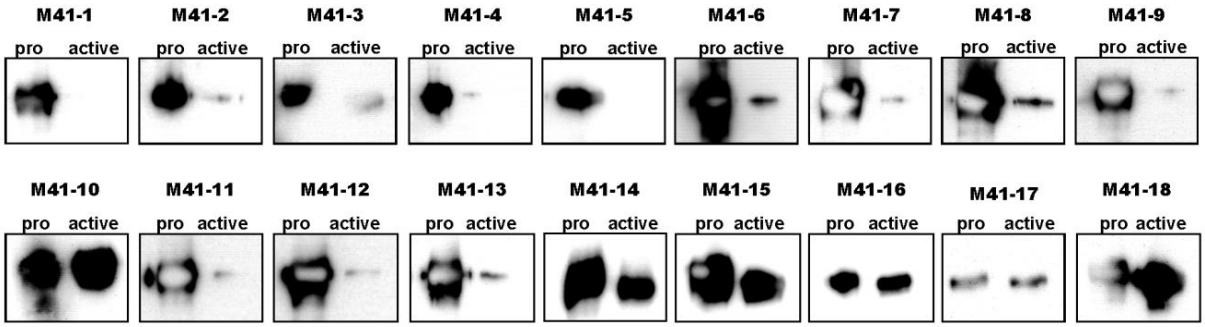

Figure 18: Western blot analysis of recombinant human meprin α using mAb produced by the hybridoma clones M41-1 to M41-18.

0.5 µg pro and active meprin α was separated by SDS-PAGE under reducing conditions and subsequently transferred to PVDF membrane. Supernatants of the hybridoma cells M41-1 – M41-18 were used for detection of recombinant human meprin α.

Three of the eighteen positive hybridoma cell lines M41-5, M41-14, and M41-15 containing secreted meprin α mAb were selected for further analyses. To confirm that selected antibodies specifically detect meprin α, they were tested for cross-reactivity with other astacin proteases. As deduced from the Western blot (Fig. 19), none of the tested mAbs cross-reacted neither with other recombinant astacin proteases, nor with the Strep-tag of promeprin α.

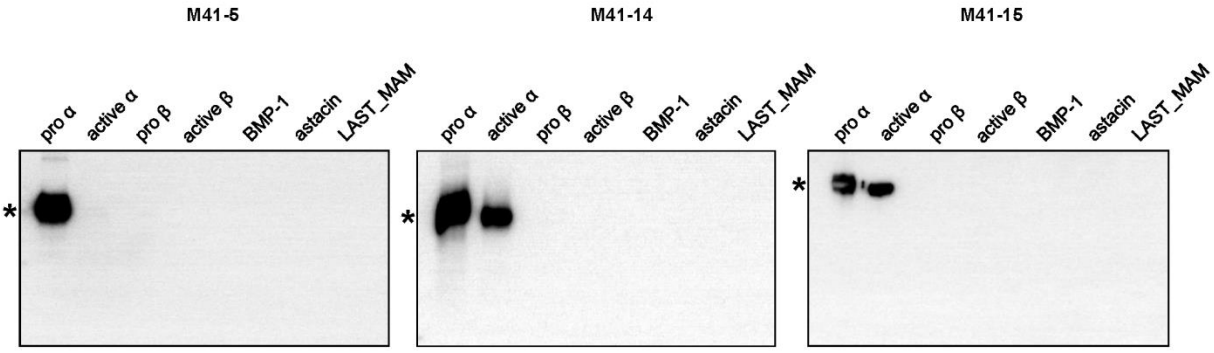

Figure 19: Cross-reactivity analysis of recombinant human meprin α using mAb produced by the hybridoma cells M41-5, M41-14, and M41-15.

0.5 µg human recombinant pro and active meprin α or meprin β, BMP-1, astacin, and the Strep-tagged LAST-MAM were separated by SDS-PAGE under reducing conditions and subsequently transferred to PVDF membrane. Supernatants of the hybridoma cells M41-5, M41-5, M41-14, and M41-15 were used for detection of the proteins. Asterisk represents the molecular weight marker band of 80 kDa.

Recently it became evident, that meprins, especially meprin α, play a role in inflammation and cancer [3]. Therefore, a specific meprin α sandwich ELISA has been established for the detection of meprin α protein concentration in human serum. Among the generated hybridoma cells, the clones M41-14 and M41-15 produced mAbs which recognized the endogenous and native meprin α (Fig. 20A, 20B). Therefore these mAbs were purified and further used to establish a meprin α specific sandwich ELISA.

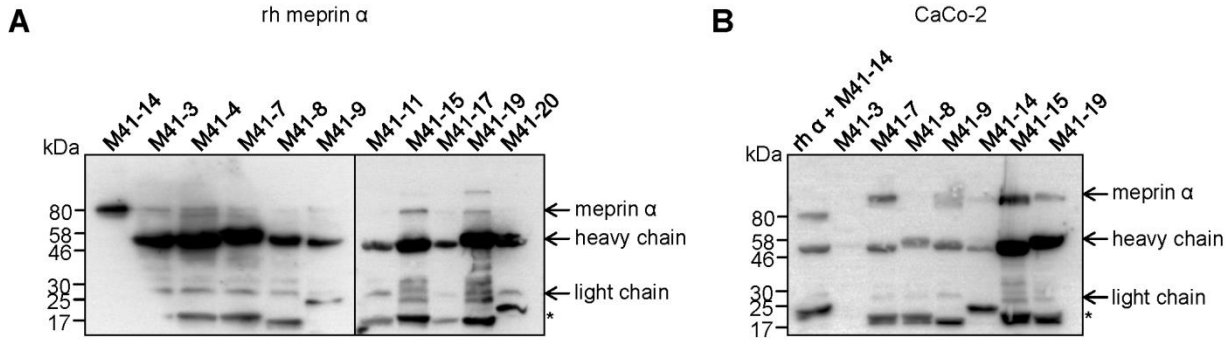

Figure 20: Immunoprecipitation of meprin α using mAbs produced by hybridoma cells.

(A) Western blot analysis of immunoprecipitated recombinant meprin α, and (B) endogenous meprin α from the supernatants of CaCo-2 cells. Proteins were separated by SDS-PAGE under reducing conditions and subsequently transferred to PVDF membrane. mAb M41-14 was used for detection of the proteins. Asterisk marks unspecific protein signals.

A sandwich ELISA specific for human meprin α was developed, where ELISA plates were coated with purified M41-15 and the antigen was detected with the biotinylated M41-14. Application of the capture antibody M41-15 and biotinylated detection antibody M41-14 enabled the detection of meprin α to a concentration of 4 ng/ml (Fig. 21A). The overexpression of meprin α is associated with many inflammatory processes [3]. Interestingly, in human sera obtained from patients suffering from rheumatoid arthritis, a chronic, inflammatory autoimmune disease, 20 ng/ml meprin α could be detected while meprin α serum levels in healthy donors were below the sensitivity of this ELISA (Fig. 21B).

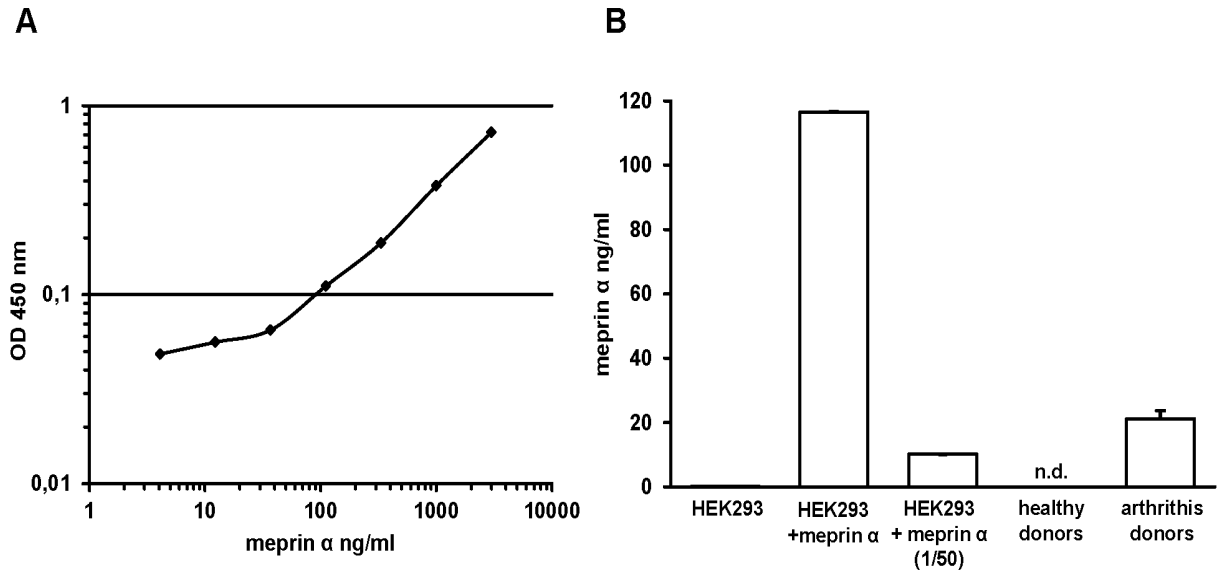

Figure 21: Sandwich ELISA using mAb M41-15 as capture antibody and biotinylated mAb M41-14 for detection of human meprin α.

96-well plates coated with 10 µg/ml of mAb M41-15 and were incubated with (A) 4-3000 ng/ml human recombinant meprin α for 2 h at RT. Biotinylated M41-14 was added at a final concentration of 1 µg/ml. The detection of biotinylated antibody has been performed using horseradish peroxidase-labeled streptavidin and BM blue as substrate. (B) 100 µl cell culture medium from HEK293 cell untransfected or transiently transfected with human meprin α or 100 µl serum of healthy or arthritis donors were applied on 96-well plates coated with 10 µg/ml of mAb M41-15. After incubation for 2 h at RT biotinylated M41-14 was added at a final concentration of 1 µg/ml and the detection has been performed using horseradish peroxidase-labeled streptavidin and BM blue as substrate.

Recently, a mass spectrometry based proteomics approach revealed increased serum and urine levels of meprin α in Kawasaki diseased patients [79]. Kawasaki disease is an acute vasculitis in children which causes inflammation in arteries throughout the body and is therefore the leading cause of heart disease in children [80]. A late diagnosis and treatment often leads to morbidity and mortality. Therefore, a sensitive ELISA for detection of meprin α in human serum or urine might represent a helpful tool for early diagnosis of Kawasaki disease disease or other inflammatory disorders.

4 Perspective

Fibrosis is a pathological accumulation of fibrillar collagen in tissue and represents a major global disease. It frequently results upon wound healing processes in almost any organ or tissue of the body [64]. The development of anti-fibrotic drugs is a major goal in biomedical research, which requires knowledge of all molecular mechanisms implicated in the massive collagen deposition in the ECM of connective tissues in fibrosis. Several post-translational key events during synthesis, maturation, deposition and degradation of fibrillar collagen can be targeted. This work demonstrates that meprin α and meprin β are involved in posttranslational modifications of collagens at different levels, by inducing of the release of procollagen from Hsp47 during the secretory pathway, by enzymatic conversion of procollagen into fibril forming molecules, and by regulating the activity of the collagen degrading enzyme MMP-1. Meprins are the first known procollagen I N- and C-proteinases *in vivo* and they induce the assembly and deposition of collagen I in skin. Regulating the activity of enzymes responsible for the maturation of procollagen is a suitable antifibrotic strategy for the therapeutic treatment of fibrosis [81]. Thus, inhibition of meprins in skin is a promising approach for the regulation of pathological collagen deposition in fibrotic skin.

In addition, directed inhibition of meprins might regulate the activity of MMP-1, the proteolytic enzyme which is responsible for the degradation of type I collagen and important target in fibrosis. In keloid lesions Hsp47 is highly up-regulated suggesting its role in the rapid and extensive synthesis of collagen in these tissues. Inhibition of meprins might reduce the secretion of collagen into the ECM and might be beneficial for the therapeutic treatment of fibrosis.

The application of proteomics helped to identify meprins as novel players in collagen assembly and to design specific inhibitor compounds to target these proteolytic enzymes *in vitro* and *in vivo*. In future, cell-culture studies and animal models will help to understand how these proteases are integrated within the protease web under physiological and pathological conditions and whether the regulation of their proteolytic activity by using small inhibitory compounds is beneficial for the therapeutic treatment of fibrosis.

5 References

[1] X.S. Puente, L.M. Sanchez, C.M. Overall, C. Lopez-Otin, Human and mouse proteases: a comparative genomic approach, Nat Rev Genet 4 (2003) 544-558.

[2] V. Quesada, G.R. Ordonez, L.M. Sanchez, X.S. Puente, C. Lopez-Otin, The Degradome database: mammalian proteases and diseases of proteolysis, Nucleic Acids Res 37 (2009) D239-243.

[3] C. Broder, C. Becker-Pauly, The metalloproteases meprin alpha and meprin beta: unique enzymes in inflammation, neurodegeneration, cancer and fibrosis, Biochem J 450 (2013) 253-264.

[4] F.X. Gomis-Ruth, S. Trillo-Muyo, W. Stocker, Functional and structural insights into astacin metallopeptidases, Biol Chem 393 (2012) 1027-1041.

[5] A. Ohler, M. Debela, S. Wagner, V. Magdolen, C. Becker-Pauly, Analyzing the protease web in skin: meprin metalloproteases are activated specifically by KLK4, 5 and 8 vice versa leading to processing of proKLK7 thereby triggering its activation, Biol Chem 391 (2010) 455-460.

[6] C. Becker, M.N. Kruse, K.A. Slotty, D. Kohler, J.R. Harris, S. Rosmann, E.E. Sterchi, W. Stocker, Differences in the activation mechanism between the alpha and beta subunits of human meprin, Biol Chem 384 (2003) 825-831.

[7] S. Rosmann, D. Hahn, D. Lottaz, M.N. Kruse, W. Stocker, E.E. Sterchi, Activation of human meprin-alpha in a cell culture model of colorectal cancer is triggered by the plasminogen-activating system, J Biol Chem 277 (2002) 40650-40658.

[8] D.A. Bergin, C.M. Greene, E.E. Sterchi, C. Kenna, P. Geraghty, A. Belaaouaj, C.C. Taggart, S.J. O'Neill, N.G. McElvaney, Activation of the epidermal growth factor receptor (EGFR) by a novel metalloprotease pathway, J Biol Chem 283 (2008) 31736-31744.

[9] G.P. Bertenshaw, M.T. Norcum, J.S. Bond, Structure of homo- and hetero-oligomeric meprin metalloproteases. Dimers, tetramers, and high molecular mass multimers, J Biol Chem 278 (2003) 2522-2532.

[10] T. Jefferson, U. Auf dem Keller, C. Bellac, V.V. Metz, C. Broder, J. Hedrich, A. Ohler, W. Maier, V. Magdolen, E. Sterchi, J.S. Bond, A. Jayakumar, H. Traupe, A. Chalaris, S. Rose-John, C.U. Pietrzik, R. Postina, C.M. Overall, C. Becker-Pauly, The substrate degradome of meprin metalloproteases reveals an unexpected proteolytic link between meprin beta and ADAM10, Cell Mol Life Sci 70 (2013) 309-333.

[11] D. Hahn, A. Pischitzis, S. Roesmann, M.K. Hansen, B. Leuenberger, U. Luginbuehl, E.E. Sterchi, Phorbol 12-myristate 13-acetate-induced ectodomain shedding and phosphorylation of the human meprinbeta metalloprotease, J Biol Chem 278 (2003) 42829-42839.

[12] J.L. Arolas, C. Broder, T. Jefferson, T. Guevara, E.E. Sterchi, W. Bode, W. Stocker, C. Becker-Pauly, F.X. Gomis-Ruth, Structural basis for the sheddase function of human meprin beta metalloproteinase at the plasma membrane, Proc Natl Acad Sci U S A 109 (2012) 16131-16136.

[13] O. Kleifeld, A. Doucet, U. auf dem Keller, A. Prudova, O. Schilling, R.K. Kainthan, A.E. Starr, L.J. Foster, J.N. Kizhakkedathu, C.M. Overall, Isotopic labeling of terminal amines in complex samples identifies protein N-termini and protease cleavage products, Nat Biotechnol 28 (2010) 281-288.

[14] J. Bien, T. Jefferson, M. Causevic, T. Jumpertz, L. Munter, G. Multhaup, S. Weggen, C. Becker-Pauly, C.U. Pietrzik, The Metalloprotease Meprin beta

Generates Amino Terminal-truncated Amyloid beta Peptide Species, J Biol Chem 287 (2012) 33304-33313.
[15] F.M. LaFerla, S. Oddo, Alzheimer's disease: Abeta, tau and synaptic dysfunction, Trends Mol Med 11 (2005) 170-176.
[16] T. Jefferson, M. Causevic, U. auf dem Keller, O. Schilling, S. Isbert, R. Geyer, W. Maier, S. Tschickardt, T. Jumpertz, S. Weggen, J.S. Bond, C.M. Overall, C.U. Pietrzik, C. Becker-Pauly, Metalloprotease meprin beta generates nontoxic N-terminal amyloid precursor protein fragments in vivo, J Biol Chem 286 (2011) 27741-27750.
[17] E. Portelius, G. Brinkmalm, A.J. Tran, H. Zetterberg, A. Westman-Brinkmalm, K. Blennow, Identification of novel APP/Abeta isoforms in human cerebrospinal fluid, Neurodegener Dis 6 (2009) 87-94.
[18] P.H. Kuhn, H. Wang, B. Dislich, A. Colombo, U. Zeitschel, J.W. Ellwart, E. Kremmer, S. Rossner, S.F. Lichtenthaler, ADAM10 is the physiologically relevant, constitutive alpha-secretase of the amyloid precursor protein in primary neurons, EMBO J 29 (2010) 3020-3032.
[19] R. Postina, Activation of alpha-secretase cleavage, J Neurochem 120 Suppl 1 (2012) 46-54.
[20] C.M. Overall, R.A. Dean, Degradomics: systems biology of the protease web. Pleiotropic roles of MMPs in cancer, Cancer Metastasis Rev 25 (2006) 69-75.
[21] J. Kanitakis, Anatomy, histology and immunohistochemistry of normal human skin, Eur J Dermatol 12 (2002) 390-399; quiz 400-391.
[22] C. Becker-Pauly, M. Howel, T. Walker, A. Vlad, K. Aufenvenne, V. Oji, D. Lottaz, E.E. Sterchi, M. Debela, V. Magdolen, H. Traupe, W. Stocker, The alpha and beta subunits of the metalloprotease meprin are expressed in separate layers of human epidermis, revealing different functions in keratinocyte proliferation and differentiation, J Invest Dermatol 127 (2007) 1115-1125.
[23] M.N. Kruse, C. Becker, D. Lottaz, D. Kohler, I. Yiallouros, H.W. Krell, E.E. Sterchi, W. Stocker, Human meprin alpha and beta homo-oligomers: cleavage of basement membrane proteins and sensitivity to metalloprotease inhibitors, Biochem J 378 (2004) 383-389.
[24] P.D. Walker, G.P. Kaushal, S.V. Shah, Meprin A, the major matrix degrading enzyme in renal tubules, produces a novel nidogen fragment in vitro and in vivo, Kidney Int 53 (1998) 1673-1680.
[25] B. Oneda, N. Lods, D. Lottaz, C. Becker-Pauly, W. Stocker, J. Pippin, M. Huguenin, D. Ambort, H.P. Marti, E.E. Sterchi, Metalloprotease meprin beta in rat kidney: glomerular localization and differential expression in glomerulonephritis, PLoS One 3 (2008) e2278.
[26] S. Weber, M.T. Niessen, J. Prox, R. Lullmann-Rauch, A. Schmitz, R. Schwanbeck, C.P. Blobel, E. Jorissen, B. de Strooper, C.M. Niessen, P. Saftig, The disintegrin/metalloproteinase Adam10 is essential for epidermal integrity and Notch-mediated signaling, Development 138 (2011) 495-505.
[27] F. Shi, J. Harman, K. Fujiwara, J. Sottile, Collagen I matrix turnover is regulated by fibronectin polymerization, Am J Physiol Cell Physiol 298 (2010) C1265-1275.
[28] K.E. Kadler, D.F. Holmes, H. Graham, T. Starborg, Tip-mediated fusion involving unipolar collagen fibrils accounts for rapid fibril elongation, the occurrence of fibrillar branched networks in skin and the paucity of collagen fibril ends in vertebrates, Matrix Biol 19 (2000) 359-365.
[29] E.G. Canty, K.E. Kadler, Procollagen trafficking, processing and fibrillogenesis, J Cell Sci 118 (2005) 1341-1353.

[30] E. Makareeva, N.A. Aviles, S. Leikin, Chaperoning osteogenesis: new protein-folding disease paradigms, Trends Cell Biol 21 (2011) 168-176.
[31] D.J. Hulmes, Building collagen molecules, fibrils, and suprafibrillar structures, J Struct Biol 137 (2002) 2-10.
[32] A. Colige, I. Vandenberghe, M. Thiry, C.A. Lambert, J. Van Beeumen, S.W. Li, D.J. Prockop, C.M. Lapiere, B.V. Nusgens, Cloning and characterization of ADAMTS-14, a novel ADAMTS displaying high homology with ADAMTS-2 and ADAMTS-3, J Biol Chem 277 (2002) 5756-5766.
[33] D.R. Hopkins, S. Keles, D.S. Greenspan, The bone morphogenetic protein 1/Tolloid-like metalloproteinases, Matrix Biol 26 (2007) 508-523.
[34] C. Moali, B. Font, F. Ruggiero, D. Eichenberger, P. Rousselle, V. Francois, A. Oldberg, L. Bruckner-Tuderman, D.J. Hulmes, Substrate-specific modulation of a multisubstrate proteinase. C-terminal processing of fibrillar procollagens is the only BMP-1-dependent activity to be enhanced by PCPE-1, J Biol Chem 280 (2005) 24188-24194.
[35] M.P. Sarras, Jr., BMP-1 and the astacin family of metalloproteinases: a potential link between the extracellular matrix, growth factors and pattern formation, Bioessays 18 (1996) 439-442.
[36] W.N. Pappano, B.M. Steiglitz, I.C. Scott, D.R. Keene, D.S. Greenspan, Use of Bmp1/Tll1 doubly homozygous null mice and proteomics to identify and validate in vivo substrates of bone morphogenetic protein 1/tolloid-like metalloproteinases, Mol Cell Biol 23 (2003) 4428-4438.
[37] D. Kronenberg, B.C. Bruns, C. Moali, S. Vadon-Le Goff, E.E. Sterchi, H. Traupe, M. Bohm, D.J. Hulmes, W. Stocker, C. Becker-Pauly, Processing of procollagen III by meprins: new players in extracellular matrix assembly?, J Invest Dermatol 130 (2010) 2727-2735.
[38] C. Becker-Pauly, O. Barre, O. Schilling, U. Auf dem Keller, A. Ohler, C. Broder, A. Schutte, R. Kappelhoff, W. Stocker, C.M. Overall, Proteomic analyses reveal an acidic prime side specificity for the astacin metalloprotease family reflected by physiological substrates, Mol Cell Proteomics 10 (2011) M111 009233.
[39] L.W. Fisher, J.T. Stubbs, 3rd, M.F. Young, Antisera and cDNA probes to human and certain animal model bone matrix noncollagenous proteins, Acta Orthop Scand Suppl 266 (1995) 61-65.
[40] C. Broder, The Metalloproteases Meprin α and Meprin β are C- and N-procollagen Proteinases resulting in an Ehlers-Danlos syndrome-like phenotype in Mep1a-/- and Mep1b-/- mice, Proc Natl Acad Sci U S A (2013).
[41] R.E. Yura, S.G. Bradley, G. Ramesh, W.B. Reeves, J.S. Bond, Meprin A metalloproteases enhance renal damage and bladder inflammation after LPS challenge, Am J Physiol Renal Physiol 296 (2009) F135-144.
[42] G.A. McQuibban, J.H. Gong, J.P. Wong, J.L. Wallace, I. Clark-Lewis, C.M. Overall, Matrix metalloproteinase processing of monocyte chemoattractant proteins generates CC chemokine receptor antagonists with anti-inflammatory properties in vivo, Blood 100 (2002) 1160-1167.
[43] C. Widmer, J.M. Gebauer, E. Brunstein, S. Rosenbaum, F. Zaucke, C. Drogemuller, T. Leeb, U. Baumann, Molecular basis for the action of the collagen-specific chaperone Hsp47/SERPINH1 and its structure-specific client recognition, Proc Natl Acad Sci U S A 109 (2012) 13243-13247.
[44] A. Trad, N. Hedemann, M. Shomali, V. Pawlak, J. Grotzinger, I. Lorenzen, Development of sandwich ELISA for detection and quantification of human

and murine a disintegrin and metalloproteinase17, J Immunol Methods 371 (2011) 91-96.
[45] K.E. Kadler, Y. Hojima, D.J. Prockop, Assembly of collagen fibrils de novo by cleavage of the type I pC-collagen with procollagen C-proteinase. Assay of critical concentration demonstrates that collagen self-assembly is a classical example of an entropy-driven process, J Biol Chem 262 (1987) 15696-15701.
[46] V. Ottani, D. Martini, M. Franchi, A. Ruggeri, M. Raspanti, Hierarchical structures in fibrillar collagens, Micron 33 (2002) 587-596.
[47] N. Suzuki, P.A. Labosky, Y. Furuta, L. Hargett, R. Dunn, A.B. Fogo, K. Takahara, D.M. Peters, D.S. Greenspan, B.L. Hogan, Failure of ventral body wall closure in mouse embryos lacking a procollagen C-proteinase encoded by Bmp1, a mammalian gene related to Drosophila tolloid, Development 122 (1996) 3587-3595.
[48] R.B. Watson, G.A. Wallis, D.F. Holmes, D. Viljoen, P.H. Byers, K.E. Kadler, Ehlers Danlos syndrome type VIIB. Incomplete cleavage of abnormal type I procollagen by N-proteinase in vitro results in the formation of copolymers of collagen and partially cleaved pNcollagen that are near circular in cross-section, J Biol Chem 267 (1992) 9093-9100.
[49] A. Colige, L. Nuytinck, I. Hausser, A.J. van Essen, M. Thiry, C. Herens, L.C. Ades, F. Malfait, A.D. Paepe, P. Franck, G. Wolff, J.C. Oosterwijk, J.H. Smitt, C.M. Lapiere, B.V. Nusgens, Novel types of mutation responsible for the dermatosparactic type of Ehlers-Danlos syndrome (Type VIIC) and common polymorphisms in the ADAMTS2 gene, J Invest Dermatol 123 (2004) 656-663.
[50] D.F. Holmes, R.B. Watson, B. Steinmann, K.E. Kadler, Ehlers-Danlos syndrome type VIIB. Morphology of type I collagen fibrils formed in vivo and in vitro is determined by the conformation of the retained N-propeptide, J Biol Chem 268 (1993) 15758-15765.
[51] C. Giunta, C. Chambaz, M. Pedemonte, S. Scapolan, B. Steinmann, The arthrochalasia type of Ehlers-Danlos syndrome (EDS VIIA and VIIB): the diagnostic value of collagen fibril ultrastructure, Am J Med Genet A 146A (2008) 1341-1346.
[52] L.P. Norman, W. Jiang, X. Han, T.L. Saunders, J.S. Bond, Targeted disruption of the meprin beta gene in mice leads to underrepresentation of knockout mice and changes in renal gene expression profiles, Mol Cell Biol 23 (2003) 1221-1230.
[53] W.M. Wang, G. Ge, N.H. Lim, H. Nagase, D.S. Greenspan, TIMP-3 inhibits the procollagen N-proteinase ADAMTS-2, Biochem J 398 (2006) 515-519.
[54] A. Page-McCaw, A.J. Ewald, Z. Werb, Matrix metalloproteinases and the regulation of tissue remodelling, Nature reviews. Molecular cell biology 8 (2007) 221-233.
[55] H.E. Van Wart, H. Birkedal-Hansen, The cysteine switch: a principle of regulation of metalloproteinase activity with potential applicability to the entire matrix metalloproteinase gene family, Proc Natl Acad Sci U S A 87 (1990) 5578-5582.
[56] E.F. Pettersen, T.D. Goddard, C.C. Huang, G.S. Couch, D.M. Greenblatt, E.C. Meng, T.E. Ferrin, UCSF Chimera--a visualization system for exploratory research and analysis, Journal of computational chemistry 25 (2004) 1605-1612.
[57] F.G. Spinale, Matrix metalloproteinases: regulation and dysregulation in the failing heart, Circ Res 90 (2002) 520-530.

[58] A.C. Newby, Dual role of matrix metalloproteinases (matrixins) in intimal thickening and atherosclerotic plaque rupture, Physiol Rev 85 (2005) 1-31.
[59] P.K. Shah, Inflammation, metalloproteinases, and increased proteolysis: an emerging pathophysiological paradigm in aortic aneurysm, Circulation 96 (1997) 2115-2117.
[60] C.E. Brinckerhoff, L.M. Matrisian, Matrix metalloproteinases: a tail of a frog that became a prince, Nat Rev Mol Cell Biol 3 (2002) 207-214.
[61] N.P. Kadoglou, C.D. Liapis, Matrix metalloproteinases: contribution to pathogenesis, diagnosis, surveillance and treatment of abdominal aortic aneurysms, Curr Med Res Opin 20 (2004) 419-432.
[62] H. Nagase, R. Visse, G. Murphy, Structure and function of matrix metalloproteinases and TIMPs, Cardiovasc Res 69 (2006) 562-573.
[63] H. Nagase, K. Brew, Engineering of tissue inhibitor of metalloproteinases mutants as potential therapeutics, Arthritis Res 4 Suppl 3 (2002) S51-61.
[64] C.Z. Chen, M. Raghunath, Focus on collagen: in vitro systems to study fibrogenesis and antifibrosis state of the art, Fibrogenesis Tissue Repair 2 (2009) 7.
[65] G.E. Crooks, G. Hon, J.M. Chandonia, S.E. Brenner, WebLogo: a sequence logo generator, Genome Res 14 (2004) 1188-1190.
[66] F. Grams, V. Dive, A. Yiotakis, I. Yiallouros, S. Vassiliou, R. Zwilling, W. Bode, W. Stocker, Structure of astacin with a transition-state analogue inhibitor, Nat Struct Biol 3 (1996) 671-675.
[67] T.A. Wynn, T.R. Ramalingam, Mechanisms of fibrosis: therapeutic translation for fibrotic disease, Nature medicine 18 (2012) 1028-1040.
[68] V.S. Lebleu, Y. Teng, J.T. O'Connell, D. Charytan, G.A. Muller, C.A. Muller, H. Sugimoto, R. Kalluri, Identification of human epididymis protein-4 as a fibroblast-derived mediator of fibrosis, Nature medicine 19 (2013) 227-231.
[69] S. Iyer, R. Visse, H. Nagase, K.R. Acharya, Crystal structure of an active form of human MMP-1, J Mol Biol 362 (2006) 78-88.
[70] E.M. Tam, T.R. Moore, G.S. Butler, C.M. Overall, Characterization of the distinct collagen binding, helicase and cleavage mechanisms of matrix metalloproteinase 2 and 14 (gelatinase A and MT1-MMP): the differential roles of the MMP hemopexin c domains and the MMP-2 fibronectin type II modules in collagen triple helicase activities, The Journal of biological chemistry 279 (2004) 43336-43344.
[71] S.W. Manka, F. Carafoli, R. Visse, D. Bihan, N. Raynal, R.W. Farndale, G. Murphy, J.J. Enghild, E. Hohenester, H. Nagase, Structural insights into triple-helical collagen cleavage by matrix metalloproteinase 1, Proceedings of the National Academy of Sciences of the United States of America 109 (2012) 12461-12466.
[72] U. Eckhard, E. Schonauer, D. Nuss, H. Brandstetter, Structure of collagenase G reveals a chew-and-digest mechanism of bacterial collagenolysis, Nature structural & molecular biology 18 (2011) 1109-1114.
[73] H. Kido, A. Fukutomi, J. Schilling, Y. Wang, B. Cordell, N. Katunuma, Protease-specificity of Kunitz inhibitor domain of Alzheimer's disease amyloid protein precursor, Biochem Biophys Res Commun 167 (1990) 716-721.
[74] M.A. Salameh, A.S. Soares, D. Navaneetham, D. Sinha, P.N. Walsh, E.S. Radisky, Determinants of affinity and proteolytic stability in interactions of Kunitz family protease inhibitors with mesotrypsin, J Biol Chem 285 (2010) 36884-36896.

[75] M. Menendez-Gonzalez, P. Perez-Pinera, M. Martinez-Rivera, M.T. Calatayud, B. Blazquez Menes, APP processing and the APP-KPI domain involvement in the amyloid cascade, Neurodegener Dis 2 (2005) 277-283.
[76] E.S. Radisky, D.E. Koshland, Jr., A clogged gutter mechanism for protease inhibitors, Proc Natl Acad Sci U S A 99 (2002) 10316-10321.
[77] J. Hoffmann, C. Twiesselmann, M.P. Kummer, P. Romagnoli, V. Herzog, A possible role for the Alzheimer amyloid precursor protein in the regulation of epidermal basal cell proliferation, Eur J Cell Biol 79 (2000) 905-914.
[78] C. Kummer, S. Wehner, T. Quast, S. Werner, V. Herzog, Expression and potential function of beta-amyloid precursor proteins during cutaneous wound repair, Exp Cell Res 280 (2002) 222-232.
[79] A. Kentsis, A. Shulman, S. Ahmed, E. Brennan, M.C. Monuteaux, Y.H. Lee, S. Lipsett, J.A. Paulo, F. Dedeoglu, R. Fuhlbrigge, R. Bachur, G. Bradwin, M. Arditi, R.P. Sundel, J.W. Newburger, H. Steen, S. Kim, Urine proteomics for discovery of improved diagnostic markers of Kawasaki disease, EMBO Mol Med 5 (2013) 210-220.
[80] J.C. Burns, H.I. Kushner, J.F. Bastian, H. Shike, C. Shimizu, T. Matsubara, C.L. Turner, Kawasaki disease: A brief history, Pediatrics 106 (2000) E27.
[81] C.Z. Chen, Y.X. Peng, Z.B. Wang, P.V. Fish, J.L. Kaar, R.R. Koepsel, A.J. Russell, R.R. Lareu, M. Raghunath, The Scar-in-a-Jar: studying potential antifibrotic compounds from the epigenetic to extracellular level in a single well, Br J Pharmacol 158 (2009) 1196-1209.

6 Appendix

6.1 Abbreviations

ADAM	a disintegrin and metalloprotease
ADAMTS	a disintegrin and metalloprotease with thrombospondin motifs
AD	Alzheimer's Disease
APMA	p-aminophenylmercuric acetate
APP	amyloid precursor protein
Aβ	amyloid β peptide
BACE1	β-site-APP-cleaving-enzyme
BCA	bicinchoninic acid
BMP-1	bone morphogenetic protein 1
b	bases
BSA	bovine serum albumin
°C	degree celsius
CaCo-2	Caucasian colon adenocarcinoma cells
C-	carboxy-
cDNA	complementary DNA
CP	C-propeptide
C-telo	C-telopeptide
Da	dalton
dH_2O	distilled water
DMEM	Dulbecco Minimal Essential Medium
DMSO	dimethyl sulfoxide
DNA	desoxyribonucleic acid
Dnp	2,4-Dinitrophenyl
DTT	dithiothreitole
DR6	death receptor 6
E2	conserved region of the central APP domain
ECM	extracellular matrix
EGF	Epidermal Growth Factor
ELISA	enzyme linked immunosorbent assay
ER	endoplasmic reticulum
FCS	fetal calf serum
h	hours
HaCaT	human adult low calcium high temperature keratinocytes
HEK	human embryonic kidney
Hsp	heat shock protein
I	inserted
k	kilo

KLK	kallikrein
KPI	Kunitz protease inhibitor
l	liter
LEKTI	Lympho-epithelial Kazal-type-related inhibitor
M	molar
Mab	monoclonal antibody
MAM	meprin A5 protein, receptor tyrosine phosphatase μ
Mca	7-Methyloxycoumarin-4-yl) acetyl
MDCK	Madin-Darby Canine Kidney Epithelial
MEF	mouse embryonic fibroblasts
Mep	meprin
meprin	metalloprotease from renal tissue
min	minute
MMP	matrix metalloprotease
mRNA	messenger RNA
mTld	mammalian tolloid
n	nano
N-	amino-
Np	N-propeptide
N-telo	N-telopeptide
PAGE	polyacrylamide gel electrophoresis
PBS	phosphate buffered saline
PCPE-1	procollagen 1 C-proteinase enhancer
PCP	procollagen C-proteinase
PCR	polymerase chain reaction
PICS	proteomic identification of protease cleavage sites
PNP	procollagen N-proteinase
PVDF	polyvinylidene fluoride
rpm	rotations per minute
s	soluble
SDS	sodium dodecyl sulfate
sec	second
SLPI	secretory leukocyte protease inhibitor
TAILS	terminal amine isotopic labeling of substrates
TIMP	tissue inhibitors of metalloproteases
TRAF	tumor-necrosis-factor-receptor associated factor
Tll	toll-like
U373	glioblastoma-astrocytoma cells
WT	wild-type
μ	mycro

Declaration of Authorship

I hereby confirm that I have authored this dissertation independently and without use of other than the indicated resources, and that this thesis has not been submitted to any other university for any academic degree.

Kiel, August 2013

_____

Claudia Broder